A thesis submitted in partial fulfillment
of the requirements for the degree of

Bachelor of Science

in

Applied Physics

Author:	Maarten Roelofsen
Student ID:	5874114
Supervisor:	Akira Endo
Second examiner:	Stephan W.H. Eijt
Daily supervisor:	Leon G. G. Olde Scholenthuis
Project duration:	21 April 2025 – 17 July 2025

TU Delft Delft University of Technology

Mekelweg 4, 2628 CD Delft, The Netherlands

Abstract

In the quest to create a 3D map of the universe, TU Delft recently started research on a Terahertz Integral Field Unit with Universal Nanotechnology or TIFUUN. These integral field units contain up to 217 spectrometer pixels (spaxels). Kinetic inductance detectors (KID) are dominating the area coverage of a spaxel. Reducing their size, allows for more spectral channels (called voxels), resulting in a higher spectral resolving power. A new type of KID showed up, which incorporates a parallel plate capacitor with a dielectric layer, significantly reducing the required space per component compared to the current state of the art. The performance of this capacitor is compromised by two-level system (TLS) noise in the dielectric layer. Previous literature made suggestions on what material characteristics influence TLS noise, called TLS indicators. These dielectric layers, in this case a-Si layers, are deposited in a plasma inside of an inductively coupled plasma enhanced chemical vapor deposition (ICP-PECVD) machine. Plasma emission spectra were collected, using a spectrometer and an optical fiber, during the deposition of different recipes to investigate how the plasma spectrum is related to the room temperature (RT) TLS indicators of a-Si films. Voigt profile fits were made through key emission peaks in the spectral data. The ratios between the heights of the key emission peaks in the spectral data were compared to the TLS noise indicators. No statistically significant relation was found between these ratios and TLS noise indicators. These results suggest that the plasma spectrum during film deposition is unrelated to RT TLS indicators of a-Si films. This narrows the focus for future research to other factors influencing these indicators, bringing us closer to creating low TLS noise dielectric films.

Contents

List of Figures

1. Introduction

Ever since humans walk this planet they have asked themselves the following question; What is out there? In the pursuit to solve this question, the TU DELFT started conducting research on a Terahertz Integral Field Unit with Universal Nanotechnology or TIFUUN. The TIFUUN project aims to detect light with wavelengths in the millimeter-sub millimeter range. This range is useful for studying the characteristics of gas clouds in which stars form [16]. This wavelength range is difficult to observe because it is strongly affected by atmospheric emission and absorption. Another challenge is that these wavelengths correspond to low-energy photons, which do not easily trigger electronic transitions or generate photoelectric signals. As a result, highly sensitive superconducting detectors or cryogenically cooled systems are required to detect them. The next challenge and one of the main goals of TIFUUN in this range is to generate 3D maps of large cosmic volumes with spectral information, to uncover the history of cold matter, the evolution of hot matter in galaxy clusters and the emergence of large-scale structure from those materials [11].
The integral field unit (IFU) is a 2D array of spectrometers, capable of instantaneously measuring the spectrum of all points in an image. TIFUUN hosts these IFUs, each containing up to 217 spectrometer pixels (spaxels [11]). In the instrument, one is limited by the space required for each spaxel. These spaxels consist of spectral channels. These channels serve as wavelength bins into which incoming light is divided when analyzing a signal. They consist of two components: A microstrip filter and a Kinetic Inductance Detector (KID) in series. In the limited space on the spaxel, we want to put as many spectral channels as possible to distinguish different colors of this one spaxel. As KIDs are currently dominating the area coveragoe of a spaxel, it is appealing for researchers to look at possibilities to minimize the amount of space required for these KIDs.
Currently, these channels use CPW KID's which are very long, about 4000 μm, taking up much space per channel. Recently, a new technique has been studied [6]. This technique reduces the amount of space required for the KID component. This is called a Parallel Plate Capacitor KID or PPC KID. These PPC's require the introduction of an intermediate layer in between the two parallel plates. Either a dielectric can be introduced or a vacuum. In this case, the dielectric is researched. This is done because fabricating a parallel plate capacitor with a dielectric layer is easier, compared to using a vacuum. This is because in the case of a dielectric,

the two plates and the dielectric layer can be placed on top of each other. In a vacuum, the plates have to be spaced very precisely. The downside of using a dielectric is that it introduces losses and noise. [8]
Noise reduces the performance of the PPC KID. It does this through a lower Signal-to-Noise ratio (SNR) resulting in a longer measurement time. This is because noise will eventually average out, but this will take longer if there is more noise to be averaged out. To resolve this problem, it is interesting to investigate the best deposition for this dielectric material. It is especially interesting to understand what causes certain films to be better than others.
These films are made, using an ICP-PECVD machine. In this machine a plasma is created, after which chemical vapor deposition causes the film to grow. A spectrometer is used, providing the ability to look inside of this machine. The spectra from the spectrometer supply information on what particles are present inside of the machine during the deposition. Relating the composition of the plasma during deposition to the characteristics of the film, helps understand how the perfect film can be created with the least amount of TLS noise. The problem is subdivided into two main questions. Those questions are:

1. Is it possible to isolate and identify spectral emission lines inside of an ICP-PECVD during an a-Si deposition?

2. What is the relation between the spectrum of the plasma during the a-Si deposition and noise indicators?

In section 2 all the theory required to answer these question will be discussed. In section 3 the methodology will be explained, after which in sector 4 the results will be showcased and discussed. With these results, the research questions will then be answered in the concluding sector 5 and future recommendations will be made.

2. Theory

2.1 MKID

The integrated superconducting spectrometer used by the Terahertz Sensing Group consists of three main components. These components are an antenna, capturing light, a microstrip filter and an MKID. These components work together on the integrated superconducting spectrometer to tell the user exactly what wavelengths it captures.

A Microwave Kinetic Inductance Detector (MKID) is a type of superconducting resonator. At sufficiently low temperatures, in the superconducting strip on these MKID's, electrons can engage in a paired state with an energy lower than the fermi energy. At this low energy state, these electron pairs become bound. These pairs are called Cooper pairs as this behavior was first described by Leon Cooper [5]. If the light, which passed through the microstrip filter, hits these Cooper pairs, they can break their bond. After this bond has been broken, two quasi-particles are left behind. One might recognize similarities between this working principle and that of a semiconductor. What makes this technique interesting is the low energy required for breaking these cooper pairs. For example, Aluminium as a superconductor has an energy gap of about $3.4 \cdot 10^{-4}$eV, whereas a normal semiconductor usually has an energy gap around 1 eV. A lower energy gap means that the superconducting element is sensitive to electromagnetic waves with longer wavelengths and thus lower energies. This enables the detection of long, low energetic cosmic radiation. The creation of these quasi-particles causes a change in the kinetic inductance. As the resonant frequency of the MKID depends on the kinetic inductance, there is now a small change in the resonant frequency.

Now all these elements are to be put together to make sure one can retrieve useful information from these MKIDs. An input signal consisting of all frequencies is sent along the end of the MKIDs (See figure 2.1). If an electromagnetic wave, from this input signal, passes by the end of an MKID and has the exact same frequency as the resonant frequency of the KID, the light shorts through the MKID. This causes a dip in the readout signal at exactly this frequency.

Now there is one vital last step to be made to retrieve information out of these dips. If the captured light which goes into the MKID passes through a microstrip filter and breaks cooper pairs, this causes a shift in the resonant frequency of an

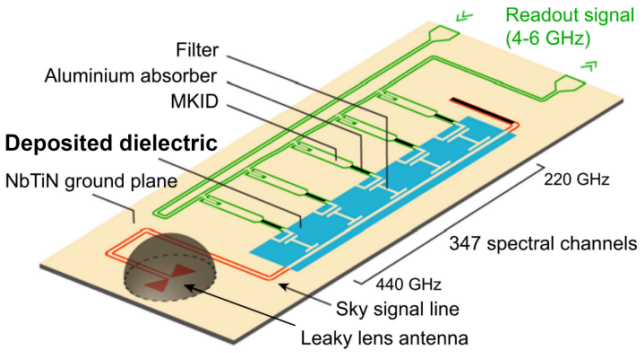

Figure 2.1: *Schematic [17] of the DESHIMA 2.0 integrated superconducting spectrometer. The radiation couples to a leaky lens antenna and travels through the sky signal line before it reaches the microstrip filter bank which includes the deposited dielectric. The MKIDs are simultaneously read out by frequency multiplexing using microwave electronics*

MKID. This causes a shift in the dip in the readout signal. The frequency at which there was a shift and the magnitude of the shift are the keys to understanding what kind of light is captured by the antenna.

2.2 Resonators

Resonance is a phenomenon in physics, which is known as a relatively large selective response of a vibrating system in phase with an external applied oscillatory force [2]. It is one of the key phenomena on which the working principle of MKIDs rely. In an MKID, a selection of resonators can be used. For the purpose of this thesis, one is of particular interest. This is the parallel plate capacitor as it requires a the least amount of space. Other types of resonators are the coplanar waveguide KID, (CPW KID) interdigitated capacitor KID (IDC KID), Hybrid KID and Lumped Element KID (LE KID). We will first discuss the CPW KID, which is the current state of the art for the DESHIMA spectrometers, shown in figure 2.1. Then we will look at the PPC KID, which could replace these CPW KIDs in the TIFUUN spectrometer array.

2.2.1 Coplanar waveguide resonators

A coplanar waveguide consists of a center conductor, through which the signal runs, and two ground planes on either side. These are all placed on the same substrate. The electric field originating from the central line terminates on the adjacent ground planes. The magnetic field forms loops around the central line. As return flows in the ground planes also form loops, these create close loops together. This causes both the electric field and magnetic field to stay confined in between the ground planes. This is what makes these waveguides very useful as a conductor, especially in the MKIDs as there are few fields escaping which could interfere with other electronics or use up signal strength. It is important to

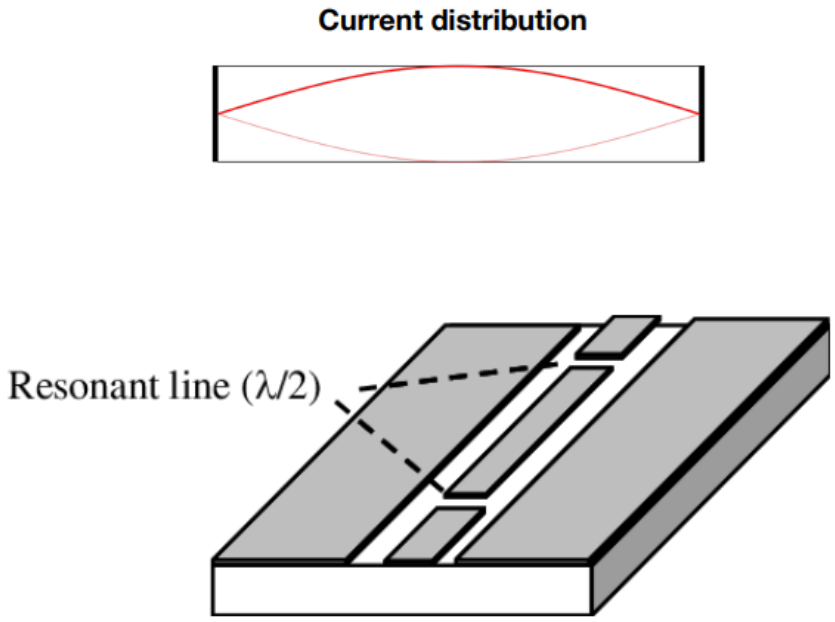

Figure 2.2: *A schematic of a coplanar waveguide resonator. The two ground plates are to the left and right of the center conductor. A wave can resonate between the two insulating parts.*

understand that these CPW's can be used as resonators but are also used as just electromagnetic waveguides.
If one were to make small gaps in the center line, this creates a small conducting part trapped in between two insulating parts. If a wave is to resonate in between these two insulating parts, a wave is required with a wavelength that meets the resonant wave condition:

$$L = n \cdot \frac{\lambda}{2} \tag{2.1}$$

Here L (m) is the physical length between the insulating parts, λ (m) is the wavelength and n is a whole integer. This standing wave can now freely resonate between these two insulating ends, creating a resonator as shown in figure 2.2. This leaves the following relation:

$$f \propto \frac{1}{L} \tag{2.2}$$

This relation depicts how the frequency (Hz) is inversely proportional to the length (m) between the insulating parts. With this knowledge, one can make coplanar waveguide resonators which only allow waves to resonate which have very specific wavelengths based their length.

2.2.2 Parallel plate capacitor

A parallel plate capacitor consists of, as suggested by the name, two conductive parallel plates. These plates are separated by an insulating material. Its main

function is to store electrical energy in the electric field between these two parallel plates. Its capacitance is a measure of how much electric charge it can hold at a given voltage and is calculated as follows in a parallel plate capacitor:

$$C = \frac{\epsilon_r \epsilon_0 A}{d} \tag{2.3}$$

In this equation C (F) is the capacitance, ϵ_r is the relative permittivity of the insulating material with respect to vacuum, ϵ_0 is the vacuum permittivity (F/M), A (m^2) is the area of the plates and d (m) the separation between them. A capacitor by itself does not resonate. They only store and release electric energy. If a capacitor is combined with an inductor, a LC-circuit is created. This circuit does exhibit resonance. The energy now oscillates back an forth between the electric field of the capacitor (C) and the magnetic field of the inductor (L). This back-and-forth motion creates a resonance at a frequency which follows the following relation:

$$f \propto \frac{1}{\sqrt{LC}} \tag{2.4}$$

This relation depicts that the frequency (Hz) is inversely proportional to the square root of the inductance (H) multiplied by the capacitance (F). With this knowledge, one can make parallel plate capacitors in combination with inductors to serve as a resonator which only resonates at very specific wavelengths depending on the capacitance of the parallel plate capacitor and the inductance of the inductor as shown in figure 2.3.

2.3 ICP-PECVD

Inductively Coupled Plasma Enhanced Chemical Vapor Deposition or in short ICP-PECVD is a thin film deposition technique. In the context of this thesis it is used to create dielectric films which are to be placed in between the parallel plate capacitors. The process that takes place in the ICP-PECVD consists of multiple steps.

First, gases such as silane, ammonia or oxygen are introduced in a vacuum chamber. These gases are called precursor gases. After these gases have been introduced, a radio frequency (RF) power source energizes a coil which surrounds the chamber. The alternating current creates a varying magnetic field in the coil. This magnetic field then induces an electric field inside the chamber, which accelerates free electrons. These electrons collide with the precursor gases, knocking of electrons and forming ions. This results in an inductively coupled plasma, which is sustained by continuous RF power. An ICP-PECVD is illustrated in figure 2.4.

These now formed ions, radicals and electrons can move freely through the chamber. These particles are highly reactive. If they hit the substrate, they react, forming a thin layer.

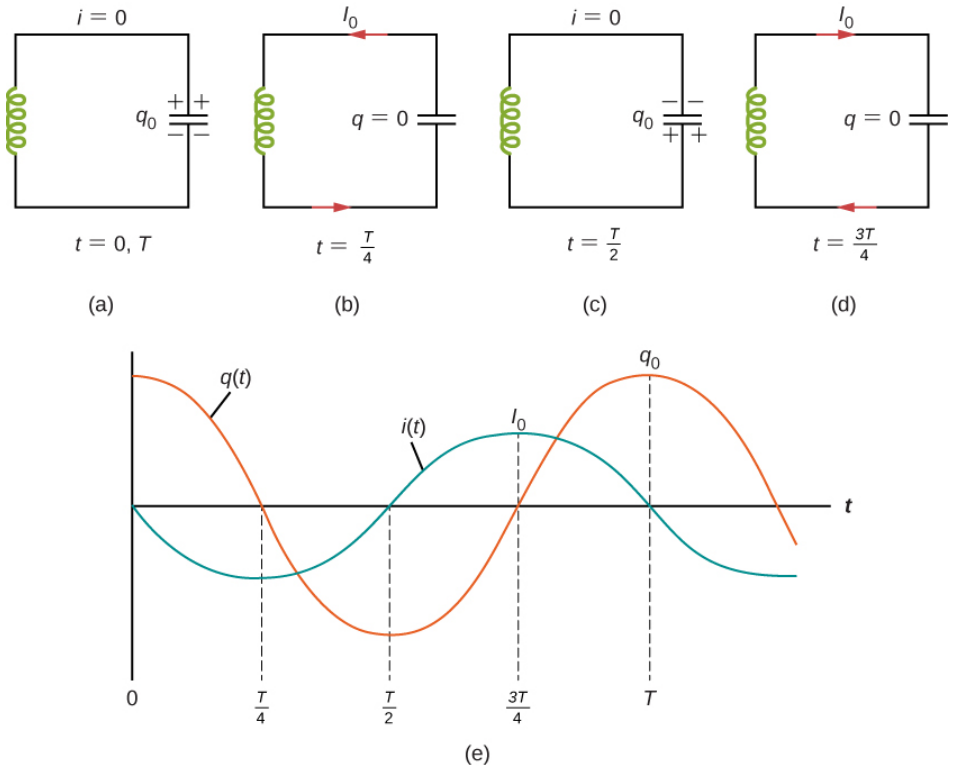

Figure 2.3: *A LC-circuit. The graph showcases how the current changes overtime as the charge in the capacitor on the right resonates over time.*

2.4 Dielectrics

A capacitor stores both electric charge as well as electrical energy by creating an electric field between two conductive surfaces. For this to work, a material is required to separate these plates and is an insulator as otherwise charge would leak and the capacitor won't be able to store this energy. If a voltage is applied between these plates we want as much charge to be stored near the plates. For this, we want a material to become polarized if a voltage is applied as this increases the capacitance and energy storage. A material that carries these properties is known as a dielectric and thus ideal for usage in a capacitor.

Dielectrics do have their downsides. First of all, through dielectric loss. Real dielectrics absorb some of the electromagnetic energy instead of storing it perfectly. This energy is then released as heat, leading to a lower efficiency as a result of dielectric loss. The cause for this dielectric loss are Two-Level System (TLS) states. In this study, the dielectric in use is an amorphous-Silicon film. Meaning that the order inside of the film is not crystalline, rather it takes on a more random order. TLS states in amorphous solids are in general not caused by impurities inside the materials, but rather emerge from these deviations away from crystalline order which characterize the amorphous state. These states allow two quantum states to be occupied simultaneously and constantly switch between them. This can happen because of interactions with electric field and thermal energy. This results in dielectric loss as these Two-Level systems can absorb

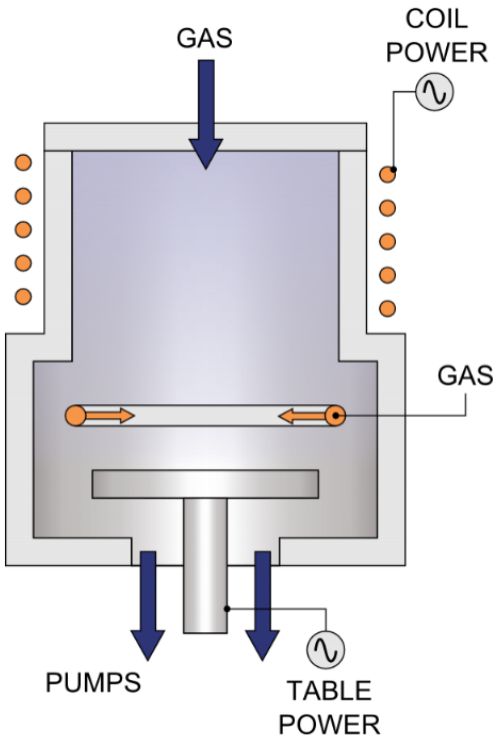

Figure 2.4: *Schematic of an ICP PECVD deposition tool [13]. The gas inlet allows various precursor gasses, with controlled gas flows, to flow into the deposition chamber. The coil is capable of initiating the plasma after which it reacts and grows a thin film on top of a wafer placed on the table. After a deposition, pumps remove the leftover gasses from the chamber.*

photons. This absorption causes the Capacitor to be less efficient. A second problem with these TLS are that it can increase frequency noise. If this TLS switching constantly occurs, it results in noise as it introduces random, time-dependent fluctuations. This noise results in a worse Signal-to-Noise ratio in the readout signal reducing the efficiency of the device. in B. Buijtendorp's thesis [4] a couple suggestions were made on what could cause this TLS noise. It was proposed that TLS's are related to the void volume fraction of a film. This indicates, in short, how much unfilled space (void) is present in a film. He suggests in chapter 2.8 that a low Void volume fraction can lead to low TLS loss. It was also suggested that hydrogen content influences the TLS noise. The Microstructure parameter was also suggested to have significant impact on TLS loss. The microstructure parameter denotes the ratio between the amount of SiH_2 and SiH configurations in the film.

2.5 Spectrometer

To check what is happening inside of the ICP PECVD, a spectrometer is utilized. This spectrometer looks inside of the chamber and gives insights on what is happening inside. It is a tool used to measure the intensity of light at different wavelengths. To measure all these different wavelengths, it has to break down light to its component colors, creating a spectrum. After which each wavelength can be analyzed individually.
First a light source emits light which falls onto a spectrometer. The light enters the spectrometer through a narrow slit. This happens to make sure a well-defined beam is received.
The light which just entered the spectrometer now gets separated in its different wavelengths. This usually happens through the use of a prism or a diffraction grating. A prism causes different wavelengths to bend by different amounts, whereas a diffraction grating reflects light in different angles based on their wavelength. Now the light is separated, this is called dispersed light. The dispersed light then hits a detector which measures the intensity of each wavelength, supplying the user with information on which wavelengths are present in the light.

2.5.1 Spectral lines

To understand how a spectrometer will eventually help identify what is happening inside of the ICP PECVD, it is important to understand how atoms can be identified by the spectrum. Every atom consists of a core consisting of protons and neutrons and an outside cloud consisting of electrons. These electrons are distributed across different layers in this cloud with a maximum of two electrons per layer. The farther away of the core a layer is, the higher the potential energy of its electrons. If an electron jumps from a higher layer to a lower layer it loses potential energy. This energy is released in the form of a photon. The energy difference between each layer and thus the energy of the emitted photon is characteristic of the atom that emitted this photon. If these photons are then captured by the spectrometer,

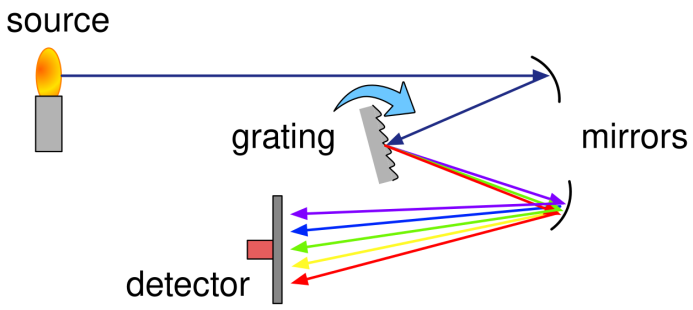

Figure 2.5: *A schematic of a grating spectrometer [9]. The light from the source is reflected on the grating after which it is dispersed. Then this dispersed light travels to the detector.*

an intensity peak appears at a very specific wavelength. This is what makes atoms identifiable by its spectral lines.

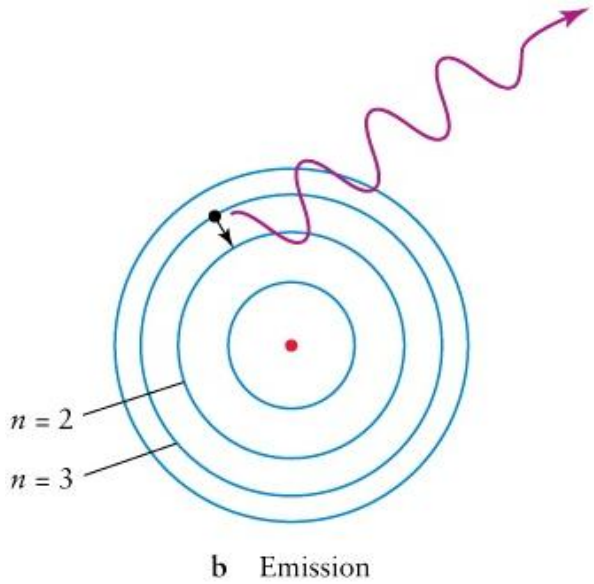

Figure 2.6: *In this schematic the emission of a photon is showcased [1]. In the figure an atom falls back from the third layer to the second layer, releasing a photon with an energy the same as the energetic difference between these two layers*

3. Method

3.1 Setup

In the introduction, the research question was subdivided into two subquestions. These are as follows:

1. Is it possible to isolate and identify spectral emission lines inside of an ICP-PECVD during an a-Si deposition?

2. What is the relation between the spectrum of the plasma during the a-Si deposition and noise indicators?

To answer these questions, firstly the setup has to be showcased. The setup consists of an ICP-PECVD Oxford plasma pro 100 in which a wafer is placed. Then a plasma is induced to start the deposition phase. On the walls of the ICP-PECVD, a glass pane is located. This glass pane allows an optical fiber connected to a SPM-M100 spectrochip spectrometer to look at the plasma inside of the ICP-PECVD. An Aluminium sheet is added through which the optical fiber is pierced, reflecting back any background light possibly interfering with the light coming from the plasma. The spectrometer shows the spectrum as received by the optical fiber. This schematic of the setup is showcased in figure 3.1. . To real setup is showcased in figure 3.2. With this setup, the research can be conducted. The research consists of a quantitative analysis of the data collected by the spectrometer during a-Si depositions of different recipes. Every recipe uses different input parameters for the ICP-PECVD machine, resulting in different depositions of a-Si and thus different spectra (see figure 3.3). The spectrometer has the exact same settings during every deposition, leading to consistent data retrieval. The spectrometer has 4 settings. Those are its range of interest (ROI), telling the spectrometer to only read and process a specific rectangular area of the sensor rather than the full image. This setting uses arbitrary units ranging from 0 to 900 and is set at an ROI of 435. At this ROI the spectrometer shows the highest intensity peaks of the spectrum during deposition in comparison to other ROI's. The width of the ROI is set to a maximum of 30, to capture as much incoming light from the deposition as possible. The spectrometer also contains the exposure time in milliseconds, which is defined as the duration over which the sensor collects light before converting it to a digital signal. This is set at

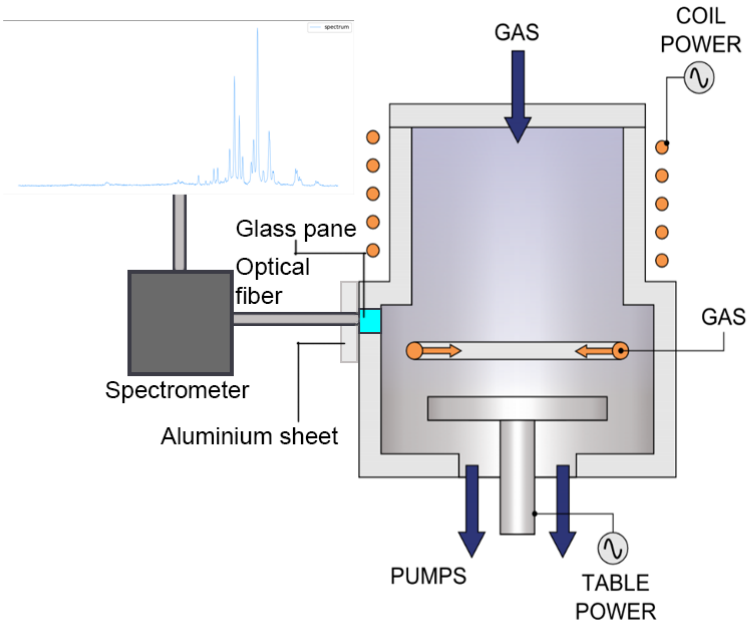

Figure 3.1: *This figure shows a schematic of the setup used for this research [13]. A coil is used to generate a plasma. Inside of the ICP-PECVD a plasma is formed during the deposition phase. An optical fiber connected to a spectrometer, which looks through a glass pane inside of the ICP-PECVD chamber. This spectrometer is connected to a computer which saves the data from the spectrometer and displays a spectrum.*

(a) *The Oxford Plasma Pro 100. The side observation pane is visible on the right side of the ICP-PECVD. The optical fiber connected to the spectrometer looks through this pane.*

(b) *The side observation pane through which an optical fiber connected to the spectrometer looks at the plasma during deposition. It is pierced through an aluminium sheet to remove any background light.*

Figure 3.2: *The setup used for this research.*

900 milliseconds. The gain is set at its maximum value of 32 to receive spectra with the highest intensity possible. The emission lines present in the spectra of these recipes from the spectrometer will then be compared to literature. The quantitative analysis can now be conducted, which means that multiple snapshots of the spectrometer are saved after which all this data is analyzed.

3.2 Data retrieval

At the beginning of each measurement, the ICP-PECVD is to be prepared for a-Si deposition. This is done by using a precondition wafer. When the precondition wafer is inside of the ICP-PEVCD, a precondition recipe has to be applied inside of the ICP-PECVD. After the recipe is finished, the ICP-PECVD is now ready for the desired recipe. In this study, six different recipes will be used in the ICP-PECVD in the EKL cleanroom 100 in Delft. These recipes are the same as used by J. Heeringa in his master thesis [7]. He has conducted research on how different recipes in the ICP-PECVD determine the material characteristics of the produced films. Those recipes are displayed in figure 3.3. During the process

Taguchi array DOE (L18)								
Rec. nr.	Table T (C)	Flow rate SiH4 (sccm)	ICP Power (W)	Table RF (W)	APC Pressure mTorr	Gas ratio (SiH4/ (SiH4+Ar))	Wafer Preparation	Pattern
1	300	15	700	50	10	75	HF Dip	−−++00+
2	300	30	300	0	15	100	HF Dip	−0−−+++
3	300	45	500	25	5	50	HF Dip	−+00−−+
4	350	15	500	50	5	100	HF Dip	0−0+−++
5	350	30	700	0	10	50	HF Dip	00+−0−+
6	350	45	300	25	15	75	HF Dip	0+−0+0+
7	390	15	700	25	15	50	HF Dip	+−−+0+−+
8	390	30	300	50	5	75	HF Dip	+0−+−0+
9	390	45	500	0	10	100	HF Dip	++0−0++
10	300	15	300	0	5	50	Argon Milling	−−−−−−−−
11	300	30	500	25	10	75	Argon Milling	−00000−
12	300	45	700	50	15	100	Argon Milling	−++++−+
13	350	15	300	25	10	100	Argon Milling	0−−00+−
14	350	30	500	50	15	50	Argon Milling	000++−−
15	350	45	700	0	5	75	Argon Milling	0++−−0−
16	390	15	500	0	15	75	Argon Milling	+−0−+0−
17	390	30	700	25	5	100	Argon Milling	+0+0−+−
18	390	45	300	50	10	50	Argon Milling	++−+0−−

Figure 3.3: *The recipes used by J. Heeringa in his Master Thesis [7]. The recipes marked blue are the ones used in this study.*

of this Bachelors End Project, J. Heeringa provided some intermediate results. These results showed that the most promising recipes were the recipes which had a Table RF of 0 W (Rec 2,5,9,10,15,16). The reason these were considered promising, was because the films created by these recipes had the lowest stress, meaning depositions would be easier. A high stress means flaking, delamination and cracking are more likely. Also bonds at the interface can weaken.
Now that the ICP-PECVD is ready and the recipes are determined, the first recipe can begin. At first, the ICP-PECVD will heat up to its desired temperatures as defined in the recipes. Then a gaseous mixture will flow into the ICP-PECVD. The deposition phase is preceded by a strike phase. During this phase, the plasma is initiated by adding power to the gaseous mixture present in the ICP-PECVD. Now, the plasma is initiated, but it is vital to wait one minute before starting to collect spectral data on the plasma present in the ICP-PECVD. This is because the plasma has to stabilize. After it is stabilized, spectral data can be captured. The spectral data of six different recipes is saved on a flash drive after which it can be analyzed. For the three recipes in which the deposition phase is preceded by an Argon milling phase, this spectral data will also be stored. These Argon spectra will help answer the question whether spectral emission lines can be isolated and identified inside of an ICP-PECVD during an a-Si deposition.

3.3 Data analysis

In Python the data is compared to the sources like the NIST database [12], which contains data on the atomic spectral lines, but also research physics articles. With this information, emission peaks in the spectra during deposition can be linked

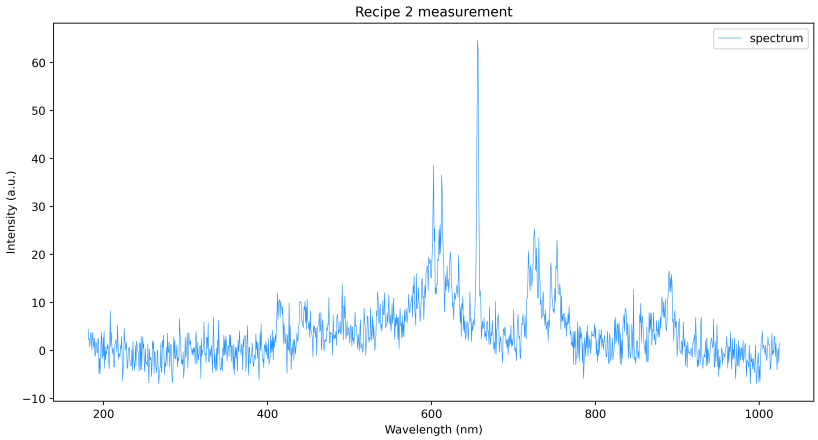

Figure 3.4: *A full-band spectrum of the a-Si plasma during the deposition of Recipe 2. Multiple peaks are visible with the highest intensity emission line at 656 nm, which is the Balmer emission line.*

to their respective ion, atom or molecule causing the peak. But before this is possible, pre-processing is done to make sure the emission lines in the spectral data are ready to be linked to their respective peaks. This means removing noise but also making representative approximations. If eventually the data can be linked to literature and peaks can be identified, the first research question will then be answered. After this, the present ions and atoms and their peaks can be linked to the material characteristics of these different recipes, as determined in J. Heeringa's Master Thesis[7]. This will eventually answer the question of what the relation is between the spectrum of the plasma during the a-Si deposition and noise indicators.

3.4 Spectral line selection

Beforehand, a decision has to be made on what atoms, ions and molecules would be of interest to this study. In a full-band spectrum during an a-Si deposition, multiple emission peaks will be visible in the spectral data, but only a couple are of use to the this study as shown in figure 3.4. For the question whether spectral emission lines can be isolated and identified inside of an ICP-PECVD during an a-Si deposition, the conclusion is made to look at 4 different atoms and molecules. These are the Balmer line H_α at 656 nm, the Silylidyne (SiH) molecule at 414 nm, the Fulcher band between 580 and 640 nm and the high intensity Argon peaks ranging from about 700 to 900 nm. This Fulcher band comes from transitions in the H_2 molecule. The Argon peaks and the Fulcher band provide a very solid set of data which can be compared to literature as on both peaks there is much known literature. The research of M. Mazzaglia on the Fulcher band will be used [10] as well as the argon spectrum obtained by A. Bogaerts [3]. The other two peaks (SiH and H_α) are used for both research questions. The Balmer line is known for its high intensity, meaning this spectral line provides a good

base to answer if spectral emission lines can be isolated and identified inside of an ICP-PECVD during an a-Si deposition. The same goes for the Silylidyne (SiH) peak. This peak provides both information on the amount of silicium in the plasma and is the easiest to detect compared to Silylene (SiH_2) and Silanide SiH_3. Both of the peaks will also come in handy to answer the question of what the relation is between the spectrum of the plasma during an a-Si deposition and noise indicators.
To relate the emission peaks in the spectral data during deposition to the noise indicators. The peak emission ratios are compared to the material characteristics of various recipes, determined by J. Heeringa. For this, the Silylidyne (SiH) and the Balmer line are used. What makes Silylidyne interesting is that it is the precursor to Si, which is what the films consists of. The Balmer line has a sharp correlation with the amount of hydrogen in the plasma. Their ratio may tell us more about the amount of hydrogen in the film. A high Silylidyne peak but a low Balmer peak suggest that the hydrogen which came from the formation of Silylidyne out of silane (SiH_4) has reacted with the film. Also the amount of hydrogen in the film has very strong impact on the TLS noise according to B. Buijtendorp [4]. The Silylidyne peak is also compared to the Fulcher band. This was done because different plasma conditions can change how hydrogen reacts. At lower pressure H_2 is less likely to split into Hydrogen atoms [15]. These atoms and molecules and their ratios will be compared to J. Heeringa's material characteristics [7].

3.5 Limitations

3.5.1 Systematic noise

During this data collection, there are a couple of limitations which have to be considered. First of all and most importantly, noise. Noise can also come from contamination on top of the used wafer. Noise can come from background light. In the room, in which the ICP-PECVD was located, the light from the strip lighting could interfere with the measurements. To minimize this effect, the optical fiber looking at the plasma pierces very tightly through an Aluminum sheet. This is done to make sure all background light will be reflected away from the fiber. The last big possible noise source considered, is inherent noise from the setup. All this noise results in a lower Signal-to-Noise Ratio (SNR), which is undesirable and can limit how well one is able to retrieve useful data from the measurements. To check if the noise is systematic, baseline measurements are done to get insights on this noise. This is done to make sure it can eventually be removed from the measured data. If the noise is purely random, in the best case, the noise cancels itself out as more measurements are done.

3.5.2 Deposition in front of the spectrometer leading to intensity decrease

Secondly, chemical vapor deposition doesn't just happen on the wafer. Via the use of an applied voltage, the movement of the ions and electrons can be influenced but there will always be some species reacting on the chamber walls.

With that comes the possibility of ions forming a thin layer on the glass pane through which the spectrometer is looking at the plasma. This will reduce the ability of the spectrometer to capture light coming of the plasma. To see what the effect of this film formation is on the measurements, a baseline measurement is done. In this measurement the same recipe will be used multiple times. This is done to make sure all the parameters stay the same. During these depositions, data is captured at systematic intervals to be able to map if intensity of the light coming through the glass pane decreases over time and at what rate it does so. If in fact the intensity does reduce over time, conclusions can't be made based on the intensity of the peak. Rather, the ratios between certain peaks has to be used to answer the questions.

3.5.3 Spectrometer resolution

A third limitation was the resolution of the spectrometer. Spectral line widths observed with this spectrometer are dominated by the instrumental broadening of about 0.625 nm. For atomic or molecular transitions with an intrinsic linewidth much narrower than this, the measured peak shape effectively reflects the instrument's line spread function, and not the physical line profile. This means that the spectrometer will be unable to resolve fine spectral features, effectively losing its ability to distinguish closely spaced transitions. Peaks in the spectral data could also get smeared out leading to an underestimate of the peak intensity.

4. Results and Discussion

4.1 Data preparation

4.1.1 Systematic noise

Results

Before the start of the measurements on the spectral data during deposition to answer the research question, potential limiting factors to the retrieval of this spectral data were listed in section 3.5. To make sure these limiting factors would not influence this retrieval, they were independently measured to make sure they could be removed from the spectral data as retrieved from the spectrometer. The first listed potential limiting factor was systematic noise. To measure the limiting factor that was systematic noise and eventually remove this from the spectral data during depositions, this systematic noise has to be mapped out. If there would be any kind of systematic noise, this would also be visible in spectra during depositions in the form of small peaks and troughs. To map this systematic noise, spectral data was collected with a spectrometer of the inside of the ICP-PECVD when there was no plasma present inside. With the use of the spectrometer 200 snapshots of the background light spectrum were successfully made. These spectra were then added together and averaged out to get the average background light spectrum in the setup and shown in figure 4.1.

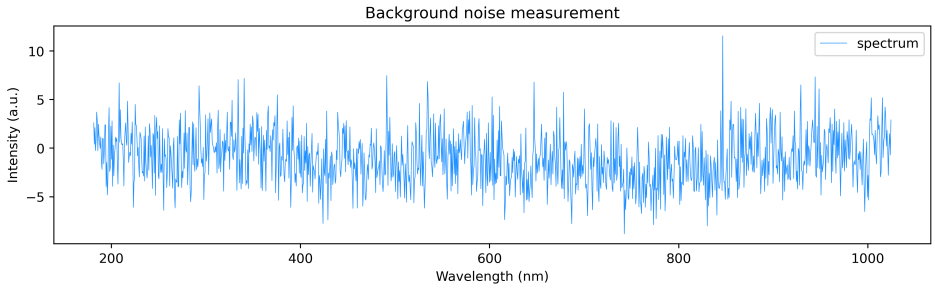

Figure 4.1: *A figure displaying the averaged out spectrum of 200 snapshots of background light spectral data when there was no deposition going on inside of the ICP-PECVD.*

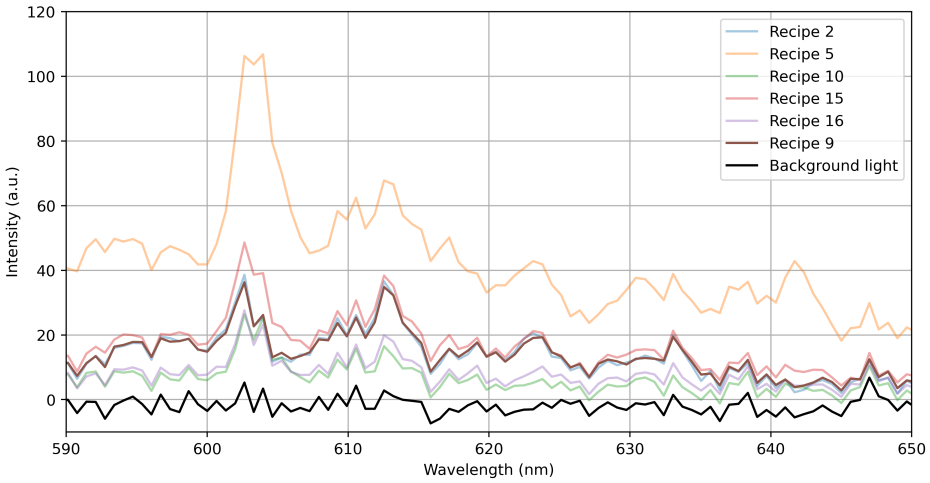

Figure 4.2: *The spectra of different recipes during deposition as well as the averaged out background light spectrum. The figure shows that peaks and troughs in the average background light spectrum appear at the exact same wavelengths as peaks and troughs in the recipes. This indicates the presence of systematic noise.*

Discussion

The reason that these spectra are added together is to make sure that if the peaks and troughs in the spectra of the background light are random, they will cancel themselves out. The averaged background light spectrum still has peaks and troughs in its intensity ranging from -7.5 to 10 arbitrary units, indicating they have not canceled themselves out. After this, it has to be checked whether this resulting average background light spectrum is a direct result from systematic noise. To check this, a plot is created showcasing all the spectra from all different recipes during deposition as well as the averaged noise spectrum. These spectra are compared in between 580 and 640 nanometers (the typical Fulcher band range) to see if the peaks and troughs in the average background light spectrum will appear at the exact same wavelengths as peaks and troughs in the spectra of the recipes during deposition, show in figure4.2. This turns out to be the case, leading to the conclusion that the intensity peaks and troughs in the averaged out background light spectrum are a direct result from systematic noise in the setup. This systematic noise spectrum can now be used to remove systematic noise from future spectral data.

4.1.2 Intensity decrease in the spectral data over time

Results

The second listed limitation to the retrieval of the spectral data was the decrease of the peak intensity in a spectrum over time during deposition. It was suggested that during deposition, the deposition would not only happen on the substrate on which the a-Si films form, but also on the glass pane through which the optical fiber connected to the spectrometer is looking at the plasma. This would cause an a-Si layer to form in front of the optical fiber, reducing the peak intensity in a

spectrum as captured by the optical fiber. To check if the peak intensity would reduce over time, the intensity during a full deposition at a specific wavelength had to be mapped out. For this purpose, the intensity of the highest point of each snapshot during a full deposition of recipe ten was chosen after which the underlying trend had to be determined. The reason the peak with the highest intensity in the spectrum was chosen, was because any present random noise would relatively have the lowest impact on the intensity of the highest peak leading to a more accurate representation of the peak height. The deposition of recipe ten was chosen as the candidate as the most snapshots were taken of this recipe during one full deposition in comparison to the other five recipes. This means that the final figure in which all the highest peak intensities over time were showcased would contain more data points, leading to a more accurate representation of the peak intensity decrease over time. A line was fitted through the peak intensities indicating whether there is a relation. As the height of the intensity of the highest peak still appeared to fluctuate in the final figure, the fit was done using a DBSCAN algorithm (See Appendix C) as shown in figure 4.3. This algorithm identified where in the final figure the highest density areas of the highest peak intensities during deposition were located. The peak intensity data points near these high density areas would be considered inliers. The highest peak intensity data points that were not near these high density areas would be considered outliers. This was done to make a fit solely through the inliers. The outliers were neglected as the goal of this fit was to model the underlying trend of a possible decrease in the intensity of the highest peak in a spectrum of which outliers are not representative.

Discussion

The final figure 4.3 indicates a clear downward trend in the peak intensity of the highest peak in a spectrum snapshot taken by the spectrometer during the deposition of recipe 10. The difference in intensity between the outliers and the fitted line through the inliers at some points shows a difference of 150 arbitrary units (a SNR of 4.67), which is very high. As the averaged out background light spectrum indicates fluctuations between -7.5 and 10 arbitrary units, noise can not be an explanation of these high intensity spikes in the maximum peak intensity over time. All of these intensity spikes also cap at the same intensity of 850 arbitrary units, the same value as the maximum intensity of the first couple snapshots of the spectrum of recipe ten. Another interesting thing to note are the last thirty measurements. The last spectral data points of the inliers have a maximum peak intensity of about 670 arbitrary units, when suddenly the last thirty data points have a maximum peak intensity near 850 arbitrary units. The fact that all thirty consecutive measurements have about the same maximum peak intensity of 850 arbitrary units, suggests something else is happening. A quick check on at what wavelengths these spectral maxima occur indicates that they all appear at the same 811 nanometers, removing the possibility of intensity spikes at other wavelengths out of the question. This raises the question of what causes these spikes in the spectral data to form during an a-Si deposition, which

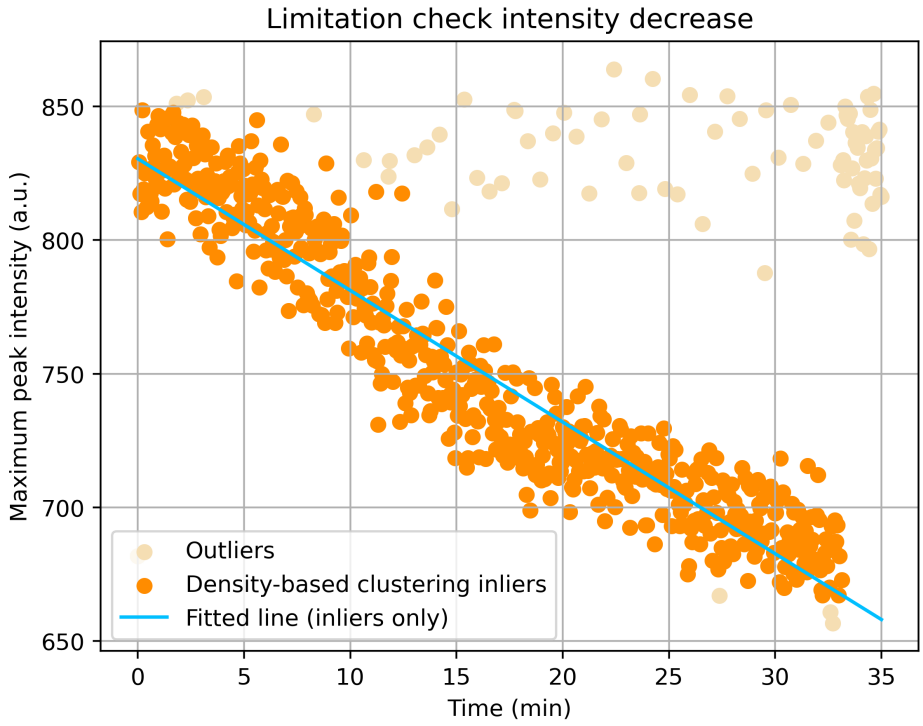

Figure 4.3: *This figure showcases how the intensity of the highest peak in a spectrum varies over time. These 660 spectral data measurements are from recipe 10 which span 35 minutes. The outliers were calculated using a DBSCAN algorithm and are not taken into account when making the linear fit.*

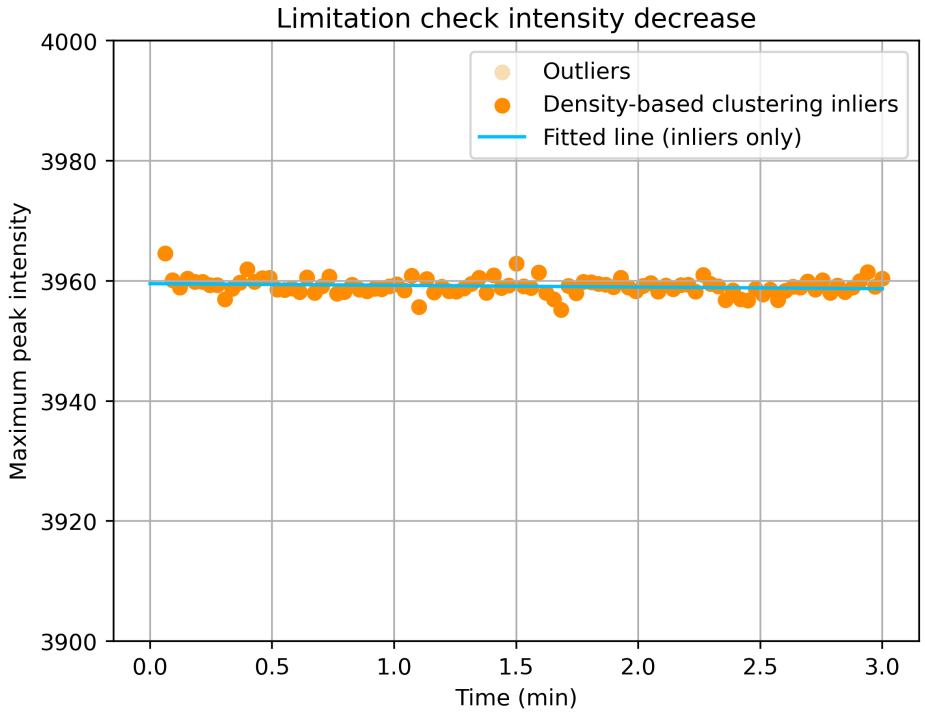

Figure 4.4: *This figure showcases how the intensity of the highest peak in a spectrum varies over time. These 150 spectral data measurements are from the Argon milling phase which span 3 minutes. The outliers were calculated using a DBSCAN algorithm and are not taken into account when making the linear fit.*

is a very interesting question to be resolved in future research.
A second check is conducted to stronger substantiate the hypothesis that the downward trend in peak intensity of a spectrum over time is caused by film formation on the glass through which the optical fiber looks at the plasma during deposition. This check is done by recreating the exact same figure as done with recipe 10, but in this case doing it for the intensity of the highest peak in the spectrum as perceived by the spectrometer during the Argon milling phase. During the argon milling phase, only Argon atoms are present inside of the ICP-PECVD. Argon is a noble gas and known for its very low chemical reactivity. This means that Argon is incapable of forming a film in front of our spectrometer. The same figure as recipe 10 is created for the Argon milling phase and the figure clearly shows no decrease in the peak intensity of highest peak in the spectra over time 4.4. It is important to note that the Argon milling phase only spans three minutes. This means that if there would be deposition of some kind during this phase on the glass, the possibility still remains that the intensity of the highest peak in a spectrum does decrease over time, only this would be hardly visible in this figure.
This confirms the hypothesis that the downward trend in peak intensity of a spectrum over time is caused by film formation on the glass through which the optical fiber looks at the plasma during deposition. This indicates that answering

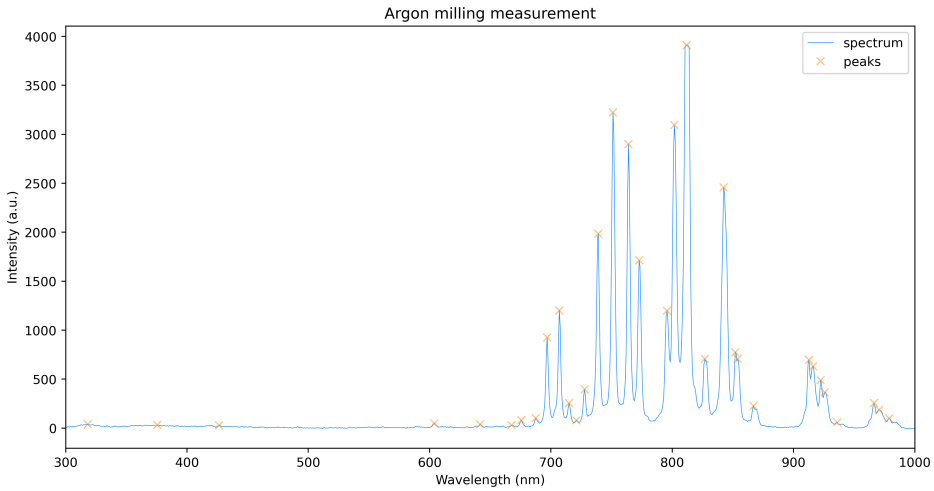

Figure 4.5: *The Argon spectrum as received by the spectrometer during the Argon milling phase. Sharp intensity peaks are visible in between 700 and 900 nanometers.*

the question on what the relation is between the spectrum of the plasma during an a-Si deposition and noise indicators can not be done based solely on the intensity of any peaks present in the spectra as received by the spectrometer. Instead, ratios between the intensity of peaks in the spectra should be used to answer the research question. Looking at ratios between the intensity of peaks in the spectra does indirectly make the assumption that the intensity peaks in the same spectra at different wavelengths decrease at the same rate.

4.2 Identifying peaks in spectral data

4.2.1 The Argon spectrum

Results

For answering the question whether emission peaks in the spectral data from the spectrometer could be linked to the species causing the intensity peak, snapshots were captured on all recipes as determined by J. Heeringa [7]. To get the denoised spectra, all six recipes were used in the ICP-PECVD and snapshots were taken of the plasma spectrum as received by the spectrometer. These spectra were added up and averaged out. After this, the systematic noise was subtracted from the averaged out spectral data set of every recipe. These were then compared to literature. The first spectral data set was the Argon spectrum. This spectrum was received by the spectrometer during the Argon milling phase prior to the deposition phase of the recipes. The Argon milling spectral data (figure 4.5) from the spectrometer showed very sharp and intense peaks in between the range of 700 to 900 nanometers. The Argon spectrum as obtained by A. Bogaerts [3] showed intensity peaks in the range between 700 and 900 nanometers (Figure 4.6) at the exact same wavelengths as the Argon spectrum as retrieved by the spectrometer (Figure 4.5).

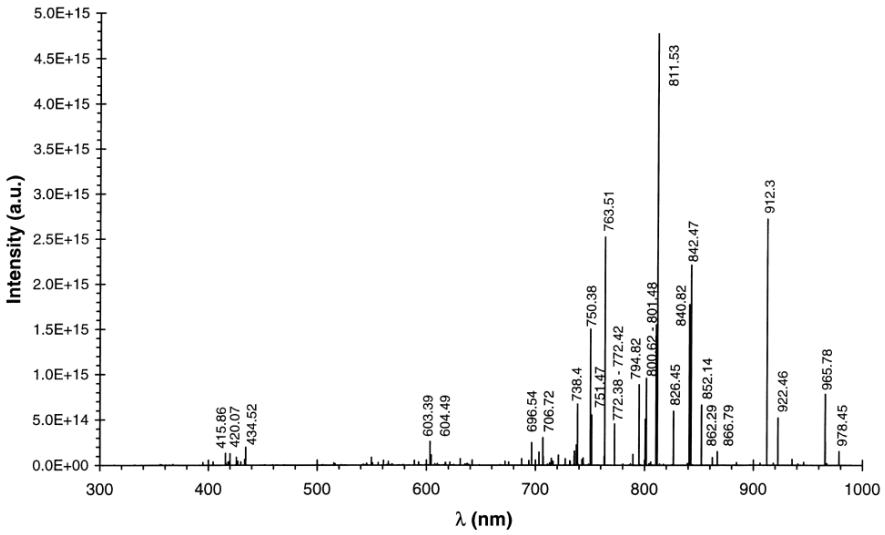

Figure 4.6: The Argon spectrum as obtained by A.Bogaerts [3]. The same sharp intensity peaks are visible in between 700 and 900 nanometers as in 4.5

Discussion

The comparison between the peaks in the Argon spectral data and the Argon literature suggests that peaks can be linked to the species causing the intensity peaks. Argon is easily identified in the spectral data as its high intensity peaks mean that the peaks have a very high Signal-to-Noise Ratio (SNR) making the peaks very easy to distinguish from noise. To further investigate if peaks can be identified from the spectral data, it is of the essence to look at wavelength regions in the spectral data in which intensity peaks are present with a low intensity peak, meaning a lower SNR. If these low SNR intensity peaks can be linked to the respective species causing the intensity peak, this further substantiates the previously made suggestion that peaks can be identified in the spectral data from the spectrometer.

4.2.2 The Fulcher band spectrum

Results

To look at low SNR intensity peaks, a wavelength range had to be compared at which peaks occur with a low SNR and a lot of research had to be done on this range. The Fulcher band was chosen and it spectral data as received by the spectrometer during deposition of the different recipes (Figure 4.7) was compared to literature on the Fulcher band as determined by M. Mazzaglia et Al. [10]. This band is a characteristic band for transitions in an H_2-molecule. The Fulcher band ranges from 590 nanometers to 650 nanometers. The spectral data of the different recipes showed low intensity peaks in this range, but all recipes did show the exact same peaks an troughs at the exact same wavelengths. The intensity peaks in the spectral data were compared to the high resolution Fulcher band spectrum as received M. Mazzaglia et Al. visible in figure 4.8.

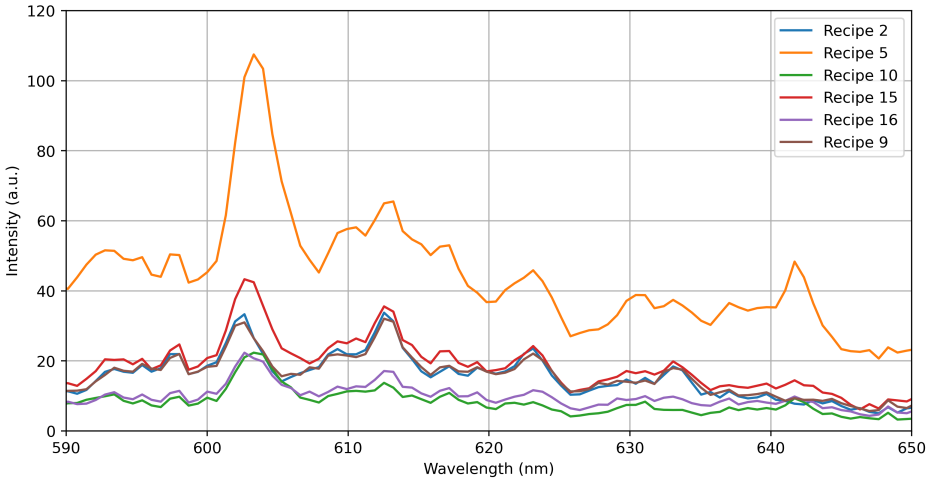

Figure 4.7: *The Fulcher band spectrum as retrieved by the data from the spectrometer. Wide peaks are visible in between the range of 590 and 650 nm.*

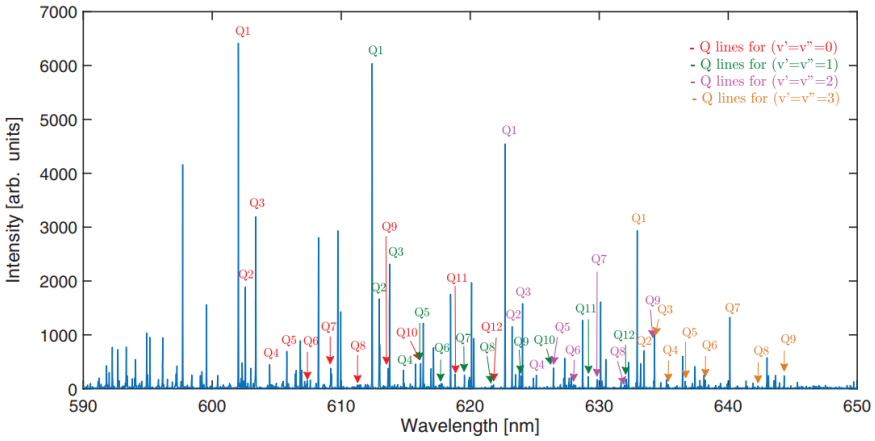

Figure 4.8: *The Fulcher band spectrum as retrieved by M. Mazzaglia et Al. [10]. Sharp peaks are visible in between the range of 590 and 650 nm at the same wavelengths as in 4.7.*

Discussion

The differences in resolution are clearly visible as the spectrometer in this study has a resolution of 0.62 nanometers where M. Mazzaglia used a spectrometer capable of reaching a resolution of 0.043 nanometers. This results in peaks in the spectrum from M. Mazzaglia being invisible in the spectrum as received by the setup used in this study during deposition. Still, the wavelengths at which intensity peaks occur in the spectrometer data from this study are located at the exact same wavelengths as the highest intensity peaks in the spectrum from M. Mazzaglia. This suggests that whilst limited by the lack of spectrometer resolution, this study is still very well capable of linking intensity peaks in the spectral data to the species causing the intensity peaks. This means that the setup and methodology used in this study is capable of answering the question on what the relation is between the spectrum of the plasma during the a-Si deposition and noise indicators.

4.3 Relating the plasma spectrum to TLS noise indicators

4.3.1 Fitting the emission peaks

Results

To answer the question of what the relation is between the plasma spectrum during deposition and TLS noise indicators, a couple elements were required. First spectral data in which peaks could be identified, a successful fit had to be done through these peak to consistently compensate for the low resolution of the spectrometer, with the error in the fit taken into account. The ratios between peaks had to be retrieved, after which data on the Noise indicators had to be acquired and compared to one another. This would help answer what the relation is between the plasma spectrum during deposition and TLS noise indicators.
As the intensity peaks in the spectral data from the spectrometer could be identified as determined in section 4.2, this research question of what the relation is between the plasma spectrum during deposition and the TLS noise indicators could now be answered. As the intensities of the peaks in the spectra decreased over time as determined in the limitation measurement section, the ratios between the intensities of key emission peaks in the spectra would be used to answer this question. To accurately calculate these emission peak ratios, a fit through the spectral data points had to be made. This was done to compensate for the low resolution of the spectrometer which received the spectral data. The height of these fits through the spectral data points near the wavelengths at which key emission peaks occur would be used to calculate these emission peak intensity ratios. The chosen fit would be a Voigt profile fit [14]. The Voigt profile fit is a convolution between a Gaussian fit and a Cauchy-Lorentz fit (see Appendix C.1). The reason this fit was chosen through our data points was that it would be the best approximation to peak broadening which could potentially occur when retrieving the spectral data from the plasma during deposition. During deposition, the particles in the plasma travel at very high speeds. This causes Doppler

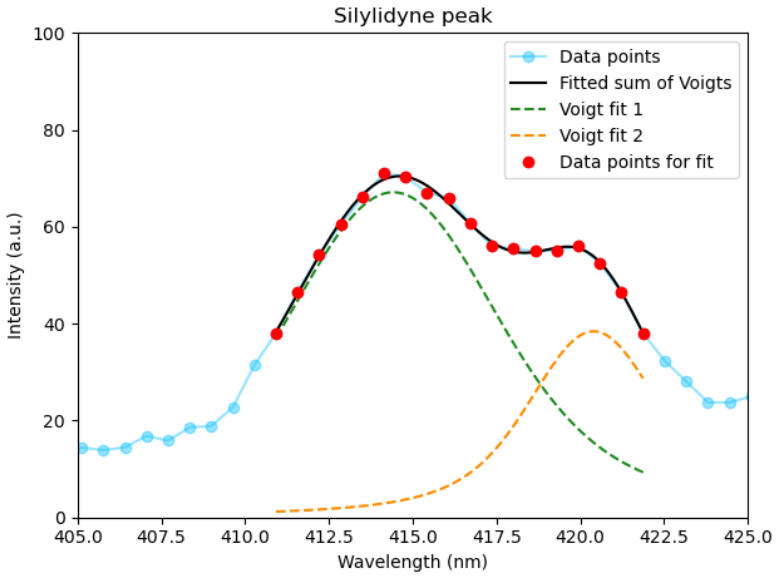

Figure 4.9: *A sum of two Voigt profiles fitted through the spectral data points of recipe five between 411 and 424 nanometers with the emission peak of Silylidyne being around 414 nm. The sum was made based on eight parameters ($\mu_{1,2}, A_{1,2}, \sigma_{1,2}, \gamma_{1,2}$), after which the individual Voigt profiles were plotted with their respective parameters.*

broadening of the emission peaks in the spectral data. A second phenomenon occurring during deposition is pressure broadening, caused by collisions between particles present in the plasma. These collisions cause a temporary shift in electron energy levels, leading to a broader emission peak. Doppler broadening is recognized by a Gaussian profile, whereas pressure broadening is recognized by a Cauchy-Lorentz profile. The Voigt profile takes both forms of broadening into account, leading to a more accurate fit through the spectral data points.
The Voigt profile was first used to calculate the ratios between the emission peak heights of the Balmer line and the Silylidyne peak during the deposition of all six recipes. For the Silylidyne peak a sum of two Voigt profiles would be used. This was done to make sure a better fit would be made through the Silylidyne emission peak as there was a second emission peak in the spectral data at 420 nm close to the Silylidyne peak, which is suspected to come from Argon ions. This is further substantiated by the fact that Argon has known peaks at this wavelength and the spectra during deposition of the recipes preceded by an Argon Milling phase showed higher intensities in the spectral data at this wavelength compared to recipes which were not preceded by an Argnon milling phase. Eventually only the peak height at 414 nm would be used for the calculation of the ratio. The Voigt profiles were then successfully fitted trough the spectral data points, also show in figures 4.9, 4.10, 4.11.

Discussion

After the Voigt profile fits through the spectral data, the sum of squared residuals between the Voigt fits and the spectral data points are calculated as a measure of the error in the Voigt profile fit (see Appendix C.2,3). Some errors are relatively

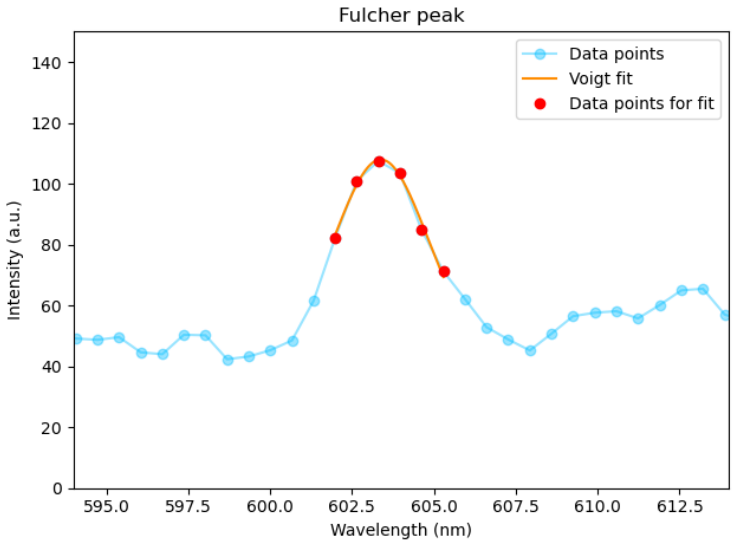

Figure 4.10: *A Voigt profile fit through the spectral data points of recipe five between 602 and 606 nanometers. With the emission peak of the Fulcher band being around 603 nm.*

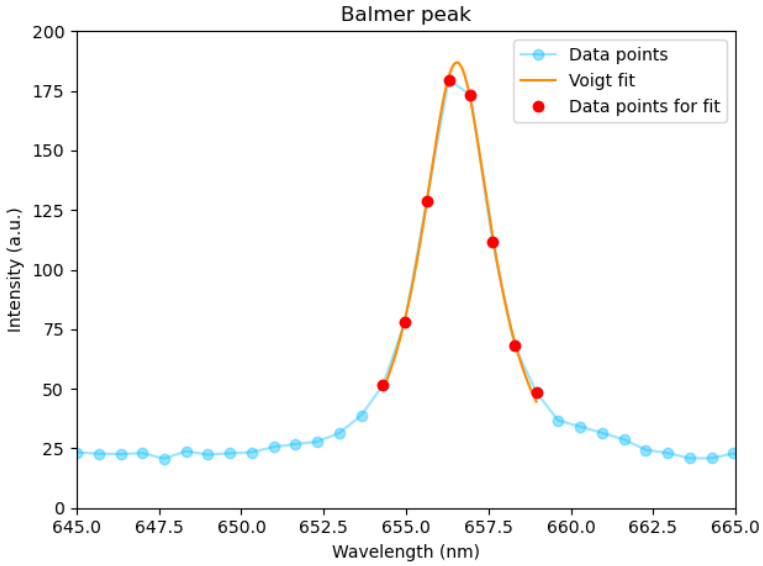

Figure 4.11: *A Voigt profile fit through the spectral data points of recipe 5 between 654 and 659 nanometers. With the emission peak of the Balmer line being around 656 nm.*

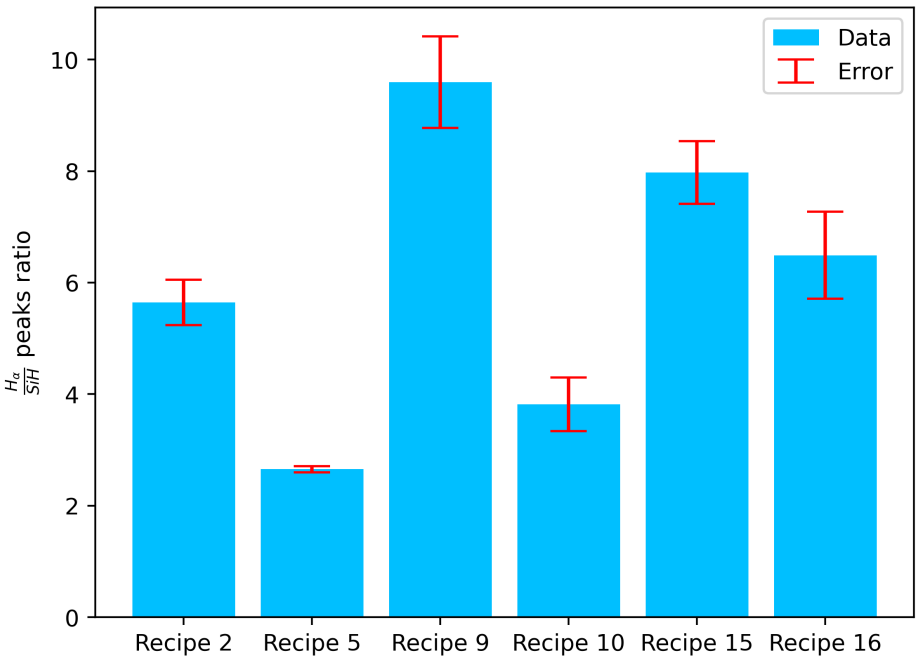

Figure 4.12: *A bar graph showcasing the ratios between the Balmer line emission peak and the Silylidyne emission peak during deposition for all recipes. The error as computed using the residuals is shown with errorbars. The exact values are shown in Appendix B.2.*

high in comparison to the ratio between the emission peaks with the highest one being Recipe ten. The opposite goes for recipe five, having the lowest error relative to its emission peak ratio as shown in figure 4.12. A possible reason for this is the difference in the input parameters for the deposition phase between the recipes. The deposition of recipe five occurs at a relatively higher pressure and temperature compared to the other recipes, resulting in emission peaks with a very high intensity causing a high SNR. The deposition of recipe ten on the other hand, happens at a very low pressure and temperature resulting in lower emission peaks with low intensities causing a lower SNR. With the now determined emission peak ratios and emission peak ratio errors, the question can be answered on what the relation is between the plasma spectrum during deposition and TLS noise indicators.

4.3.2 H_α/SiH emission peak ratio

Results

To relate the results to the TLS noise indicators, the noise indicators were used as described in J. Heeringa's Master thesis [7]. In his thesis, different material characteristics are measured. Three of the material characteristics are characterized by Buijtendorp's PHD thesis [4] as TLS noise indicators. The Noise indicators are the Hydrogen content (%) in the film, the Microstructure parameter R* (-) and the Void volume fraction (%). The other characteristics were also compared

to the ratios between the emission peaks as the data on these characteristics was available. Two of these characteristics are important for the successful fabrication of the dielectric layer. These two characteristics are Stress (MPa) and the deposition rate (nm/min). A high stress can cause the layers formed after deposition to lift off of the wafer they are placed on top of after deposition, known as delamination. Wafer stress can also cause formed films to crack or wafers can bend due to high amounts of stress. The deposition rate is a measure of how fast a film is formed during deposition. Knowing the deposition rate, results in accurate thickness control. This means that the thickness of a film can be very precisely made and reproduced. A nanometer-accurate precision in thickness is required when making parallel plate capacitors, otherwise device performance can shift. Two other characteristics were also compared to the ratios between the key emission peaks, these were the Refractive index and the Band gap (eV). In every plot a linear curve-fit was made in which the error in every ratio between the emission peaks in the spectral data was taken into account. Meaning a higher error in a calculated emission peak ratio, would result in a lower weight. A 95% confidence interval was added around the curve-fit as shown in 4.13.

Discussion

The first three figures (4.13a,4.13b, 4.13c) display the relation between the ratios between the emission peaks of the Balmer line and the Silylidyne peak from the spectral data and the TLS noise indicators. Figure 4.13a displays the relation between the Balmer and Silylidyne peak ratio and the Hydrogen content. The emission ratio data points of recipe five and recipe ten lie inside of the confidence interval of the fitted line, whereas the other data points lie outside of this confidence interval.

In figure 4.13b, displaying the relation between the Balmer and Silylidyne peak ratio and the R microstructure parameter, three recipes (5,10 and 2) lie inside of the confidence interval. Figure 4.13b, displaying the relation between the Balmer and Silylidyne peak ratio and the Hydrogen content, has a relatively wide confidence interval. Still only recipe 5 and recipe 10 lie just inside of the confidence interval. These three figures do not appear to show any kind of correlation between the emission peak ratios of the Balmer line and the Silylidyne and the TLS noise indicators. The next two figures (4.14a,4.14b) display the relation the emission peaks of the Balmer line and the Silylidyne peak from the spectral data and two useful material characteristics for potential fabrication. These two material characteristics are Stress and deposition rate as discussed in 4.3.2. Figure 4.14a displays the relation between the Balmer and Silylidyne peak ratio and the wafer stress. The emission ratio data points of recipe five and recipe two lie inside of the confidence interval of the fitted line, whereas the other data points lie outside of this confidence interval. Figure 4.14b, displaying the relation between the Balmer and Silylidyne peak ratio and the deposition rate, has three points which lie inside of its confidence interval. These are Recipe 5, Recipe 10 and Recipe 2.

The last two figures (4.15a,4.15b), displaying the relations between the emission

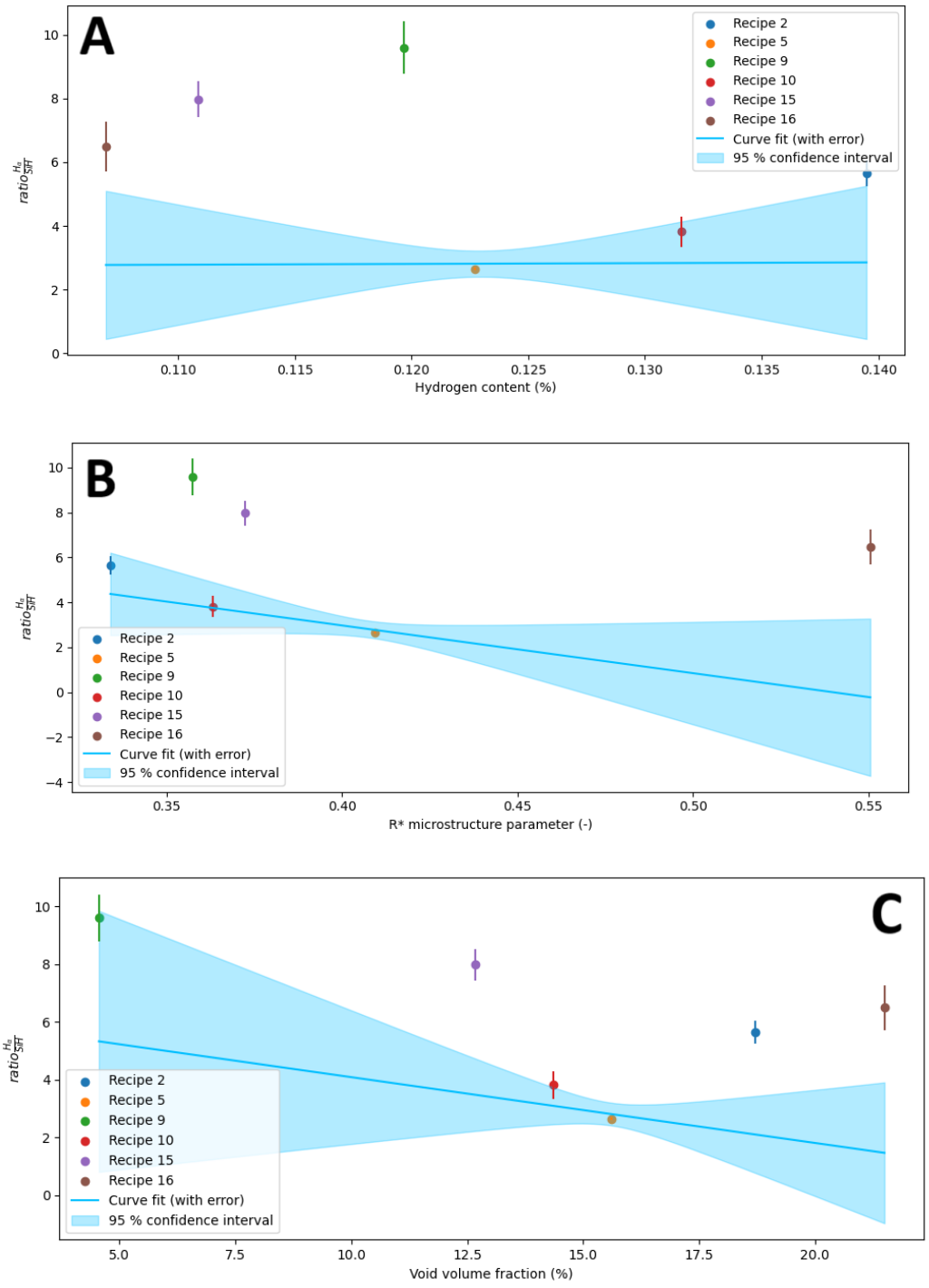

Figure 4.13: The relation between the ratios of the emission peaks of the Balmer line and the Silylidyne peak from the spectral data and the TLS noise indicators. The errors are calculated with the squared residuals and the 95% confidence interval follows from the curve fit.

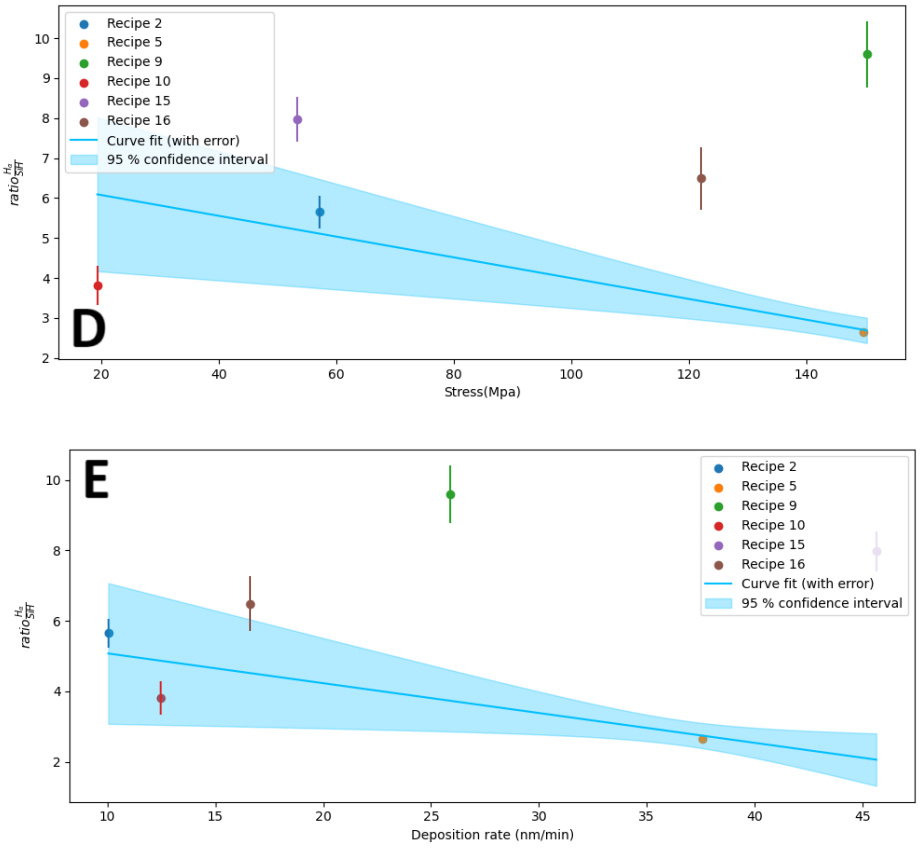

Figure 4.14: *The relation between the ratios of the emission peaks of the Balmer line and the Silylidyne peak from the spectral data and two useful material characteristics for potential fabrication. The errors are calculated with the squared residuals and the 95% confidence interval follows from the curve fit.*

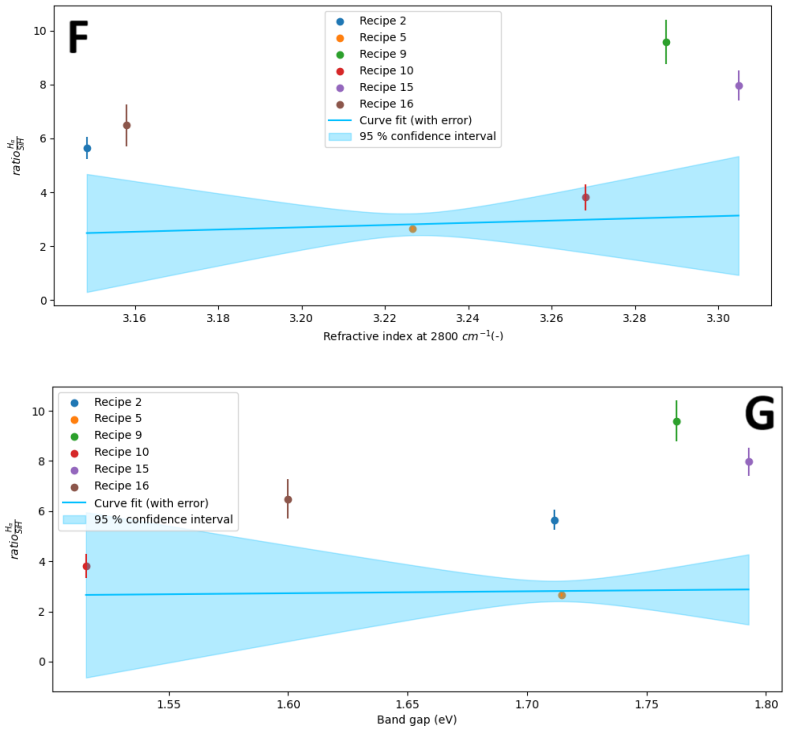

Figure 4.15: The relation between the ratios of the emission peaks of the Balmer line and the Silylidyne peak from the spectral data and the two available material characteristics, which could be useful for future research. The errors are calculated with the squared residuals and the 95% confidence interval follows from the curve fit.

peaks of the Balmer line and the Silylidyne peak from the spectral data and respectively the refractive index and the band gap, both have recipe five and ten lie inside of the confidence interval whereas the other recipes do not.
The seven figures do not appear to show any kind of correlation between the emission peak ratios of the Balmer line and the Silylidyne peak and the material characteristics, suggesting there is no simple linear correlation between the emission peak ratios of the Balmer line and the Silylidyne peak and the material characteristics. The question which arises after these results is why it is always recipes 5 and 10 which lie inside of the confidence interval. This has a simple explanation which is that the curve fit is fitted through the emission rate data points, determines the weight of these points by the size of their error bar. As recipe 5 has the smallest error (see figure 4.12), the curve fit always lies close to recipe 5. Recipe 10 happens to have a very similar emission peak ratio, making it more likely this data point lies in the confidence interval.
A possible reason causing the absence of this correlation between the emission peak ratios and the material characteristics could be plasma circumstances under which the deposition took place. The reasoning was that if a the temperature or pressure is low during deposition is low, hydrogen atoms are more likely to be in a H_2 state instead of just H compared to when both the pressure and temperature are high as shown by Cameron M Samuell [15]. To make sure no hasty conclusions were made based on the absence on a correlation in the figures displaying the ratios between emission peaks of the Balmer line and the Silylidyne peak, the same data was retrieved for the emission peak ratios between the Fulcher band and the Silylidyne peak.

4.3.3 Fulcher band/SiH emission peak ratio

Results

To eliminate the possibility of any hasty conclusions being made based on the absence on a correlation in the figures displaying the ratios between emission peaks of the Balmer line and the Silylidyne peak, the emission peak ratios between the Fulcher band and the Silylidyne peak 4.16 were compared. The ratios between the Fulcher and Silylidyne emission peaks were on average a factor 2 lower in comparison to the ratios between the Balmer and Silylidyne emission peak. The outliers in this general trend were recipe 5 and recipe 10. The ratios between the Fulcher and Silylidyne emission peaks for recipe 10 were about the same as the ratios between emission peaks of the Balmer line and the Silylidyne peaks. Whereas for recipe 5, The ratios between the Fulcher and Silylidyne emission peaks were about a factor 4 times lower in comparison to the ratios between the Balmer and Silylidyne emission peak. This substantiates that if a the temperature or pressure is low during deposition is low, hydrogen atoms are more likely to be in a H_2 state instead of just H compared to when both the pressure and temperature are high as shown by Cameron M Samuell [15]. The errors in the ratios between the Fulcher emission peaks and the Silylidyne emission peaks did not change much. This is as expected; the Fulcher band emission peak intensity has a lower intensity in comparison the the Balmer line emission peak intensity. This means

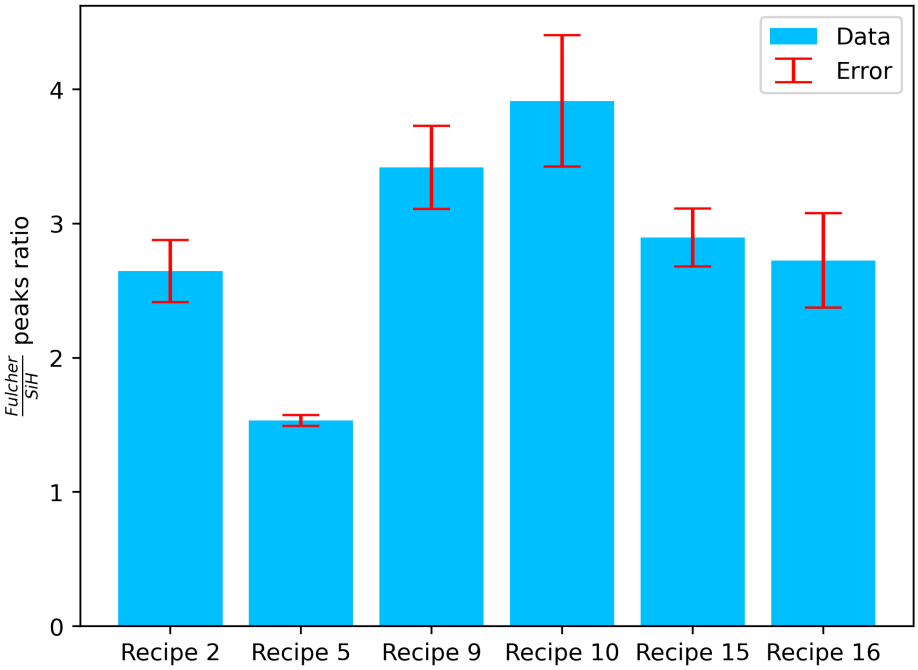

Figure 4.16: *A bar graph showcasing the ratios between the Fulcher band emission peak and the Silylidyne emission peak during deposition for all recipes. The error as computed using the residuals is shown with errorbars. The exact values are shown in Appendix B.2.*

that per definition it has a lower SNR, resulting in a worse Voigt profile curve fit through the spectral data points. This leads to a bigger sum of squared residuals, resulting in a bigger error as visible in figure 4.16.

Discussion

In the first three figures (4.17a,4.17b, 4.17c) the relation between the ratios between the emission peaks of the Fulcher band peak and the Silylidyne peak from the spectral data and the TLS noise indicators are displayed. The Hydrogen content, the R Microstructure parameter and the Void volume fraction figures all have only two recipes lie inside of the confidence interval. All of the figures have recipe 5 in the confidence interval and respectively have Recipe 16, 2 and 9 as their second recipe inside of the confidence interval.

The next two figures (4.18a,4.18b) display the relation the emission peaks of the Fulcher band peak and the Silylidyne peak from the spectral data and the two useful material characteristics for potential fabrication. These two material characteristics are Stress and deposition rate as discussed in 4.3.2. The relation between the Fulcher band peak and Silylidyne peak ratio and the wafer stress is displayed in figure 4.18a. The emission ratio data points of recipe 16 and recipe 9 lie outside of the confidence interval of the fitted line, whereas the other data points lie inside of this confidence interval. Figure 4.18b, displaying the relation between Fulchder band peak and Silylidyne peak ratio and the deposition rate, has three points which lie inside of its confidence interval. These are Recipe 5,

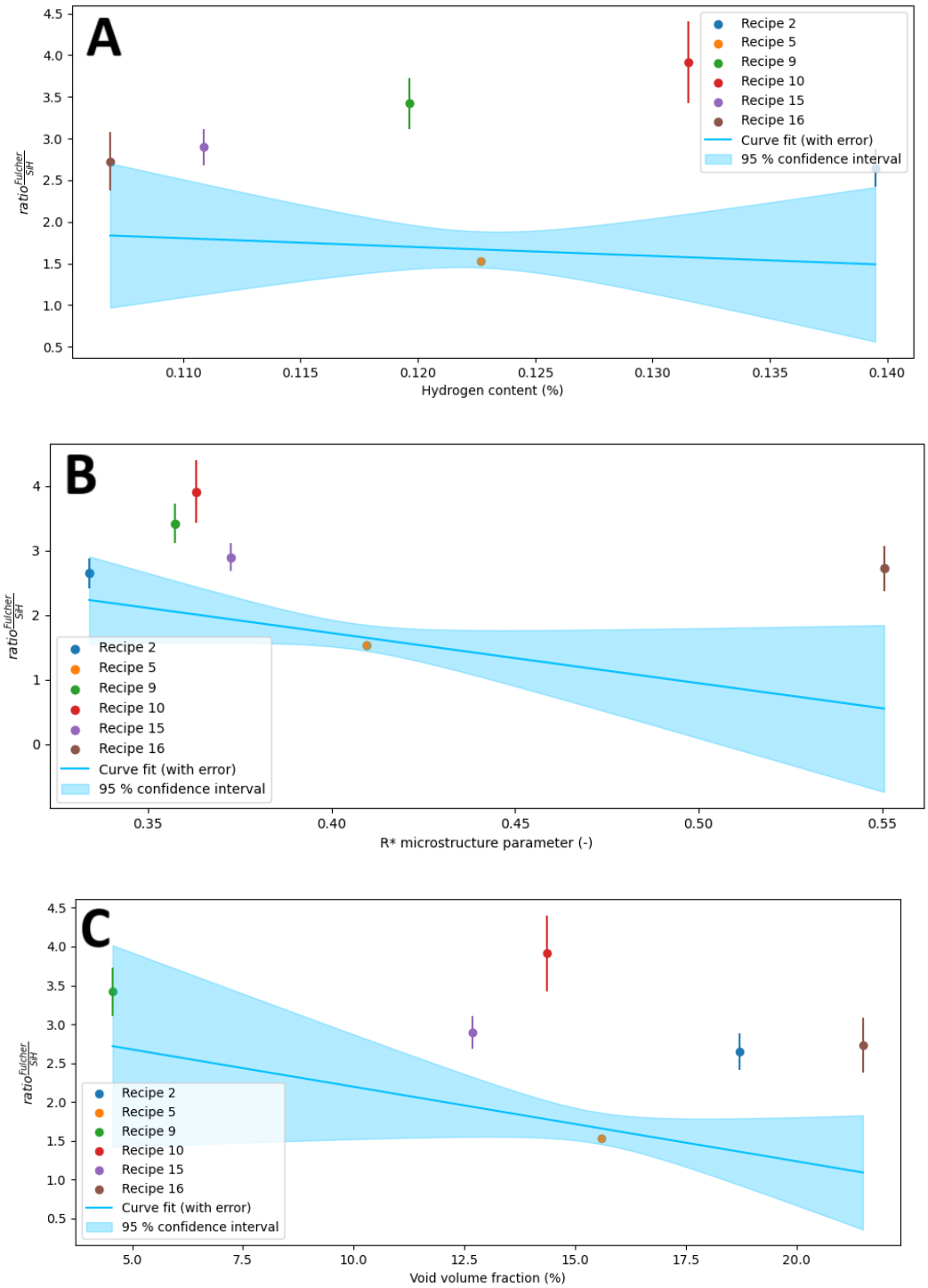

Figure 4.17: The relation between the ratios of the emission peaks of the Fulcher band peak and the Silylidyne peak from the spectral data and the TLS noise indicators. The errors are calculated with the squared residuals and the 95% confidence interval follows from the curve fit.

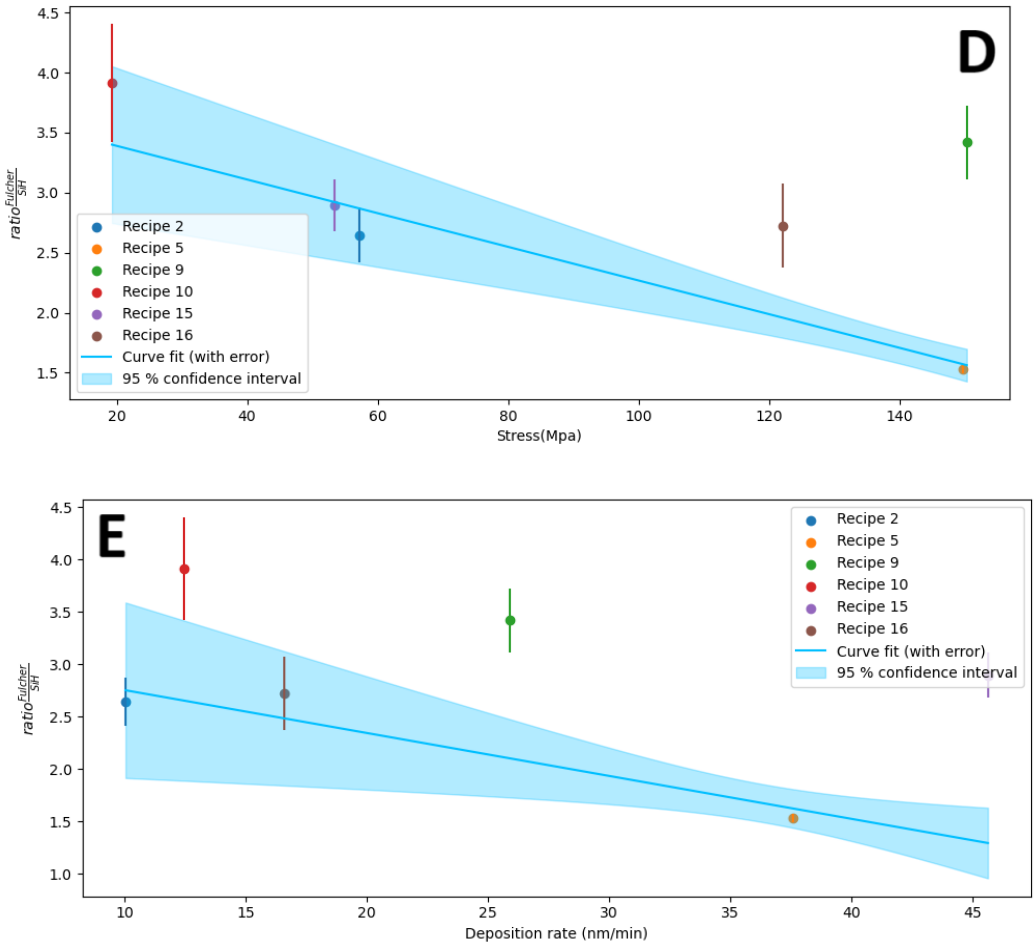

Figure 4.18: *The relation between the ratios of the emission peaks of the Fulcher band peak and the Silylidyne peak from the spectral data and two useful material characteristics for potential fabrication. The errors are calculated with the squared residuals and the 95% confidence interval follows from the curve fit.*

Recipe 16 and Recipe 2.

Then the final two figures (4.19a,4.19b), display the relations between the emission peaks of the Fulcher band peak and the Silylidyne peak from the spectral data and respectively the refractive index and the band gap, both have only recipe five lie inside of the confidence interval whereas the other recipes do not.
Although the figure displaying the relation between the emission peaks of the Fulcher band and the Silylidyne peak from the spectral data and the stress (figure 4.18a has four points lie inside of the confidence interval, this is not enough to conclude their is a correlation between the emission peaks fo the Fulcher band and the Silylidyne. Especially, since the other figure do not show a clear correlation. The figures displaying the relation between the emission peaks of the Fulcher band and the Silylidyne peak in turn further substantiate that there is no simple linear relation between the plasma spectrum and the material characteristics.

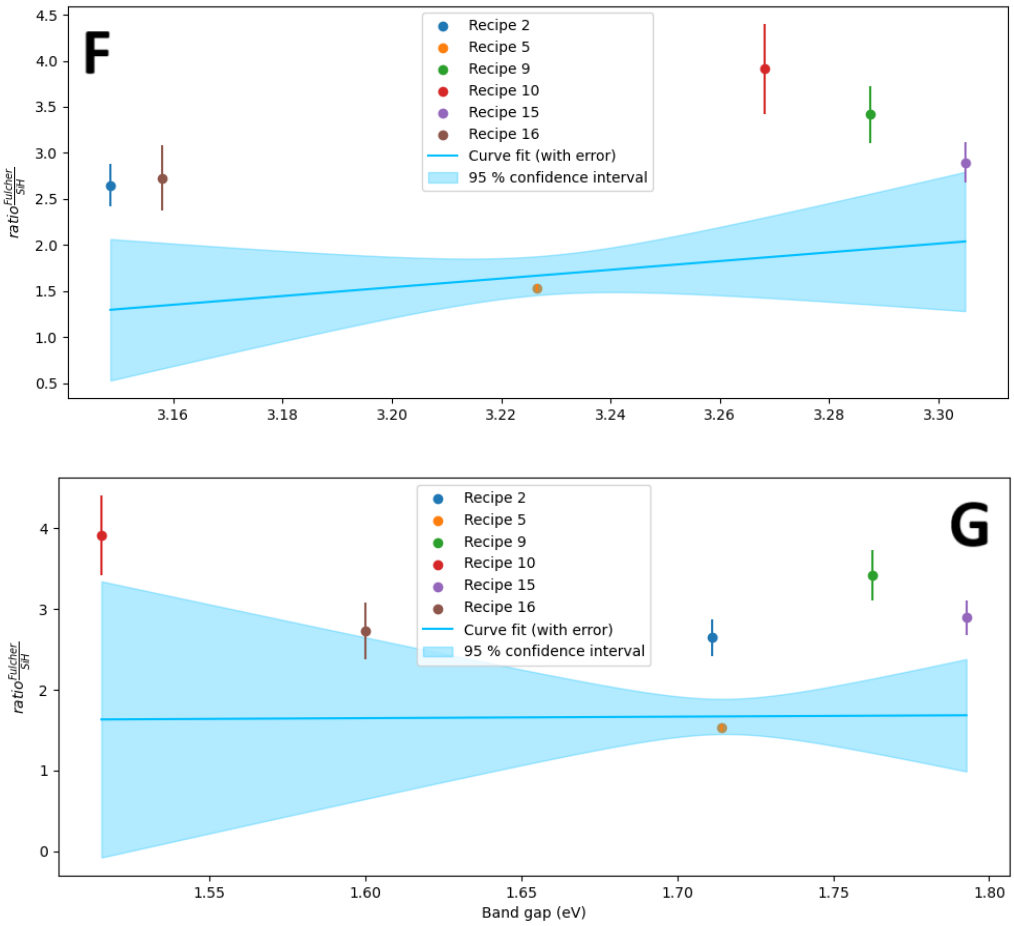

Figure 4.19: The relation between the ratios of the emission peaks of the Fulcher band peak and the Silylidyne peak from the spectral data and the three available material characteristics, which could be useful for future research. The errors are calculated with the squared residuals and the 95% confidence interval follows from the curve fit.

5. Conclusion

The first subquestion was whether key emission peaks (SiH, Balmer, Fulcher band and Argon) in the spectral data during deposition in an ICP-PECVD machine can be identified. To answer this question, background light from the room in which the ICP-PECVD was located, was removed from the spectral data. This was done by adding a reflective sheet of Aluminium during the deposition behind the optical fiber connected to the spectrometer. Then, spectral data was collected from the ICP-PECVD without a plasma present. This spectral data was then used to remove systematic noise, coming from the setup, out of the spectral data during deposition. The low resolution of the spectrometer did not appear to be a limiting factor as the resulting spectral data plots still resembled the shape of the expected plots from literary research. After comparing the finalized spectral data sets to literature, the key emission peaks of SiH, Balmer line, Fulcher band and Argon in the spectral data could be isolated and identified during an a-Si deposition inside of an ICP-PECVD.
After concluding that spectral emission lines inside of an ICP-PECVD during an a-Si deposition can be isolated and identified, the question on what the relation is between the spectrum of the plasma during an a-Si deposition and TLS noise indicators could be answered. A Voigt profile fit through the key emission peaks was used to calculate the ratios between the emission peak heights of both the SiH and the Balmer peak and the SiH and the Fulcher band peak. These peak height ratios were plotted against the TLS noise indicators. The errors in the fits were taken into account in the form of errorbars. These errors were then taken into account when making a linear curve-fit through the peak height ratios and the TLS noise indicators. A 95% confidence interval was showcased as a measure of where true values could be expected within 95% certainty from the curve fit. For every plot, more than half of the data points laid outside of this confidence interval. Ultimately leading to the conclusion that there is no simple linear relation between the plasma spectrum during deposition and TLS noise indicators.
The successful identification of peaks in the spectral data despite the low resolution of the spectrometer suggests that the setup was viable for detecting plasma features. The noise removal appeared critical to removing any noise and keeping the desired signal, emphasizing the importance of pre-processing in spectral data. The lack of a correlation between the TLS noise indicators and the

spectral data acquired after this research suggests that other factors influence the film quality or that TLS noise-indicators at room temperature aren't sensitive to variations in the ratios between the Balmer emission peak and the Silylidyne (SiH) emission peak heights and between the Fulcher band emission peak and the Silylidyne emission peak heights.
In Buijtendorp's thesis [4], it was suggested that Void Volume fraction, Hydrogen content and the R microstructure parameter have the biggest impact on the TLS noise in a dielectric. From this research it can be concluded that there is no relation between the ratio in key emission peaks in plasma spectrum and these noise indicators. This leaves the question of how a dielectric can be fabricated with the lowest amount of TLS noise unanswered. It does mean that the number of possible factors affecting the noise indicators has been reduced after this study. This brings us one step closer to creating the perfect dielectric for a parallel plate capacitor.

5.1 Future recommendations

It is important to note that the conclusion from this study that there is no correlation between the ratios in the heights of key emission peaks during deposition and TLS noise indicators does not imply that the plasma spectrum during deposition is unrelated to TLS noise indicators. From the plasma spectrum, other information can be retrieved about parameters such as the electron density in the plasma or the plasma temperature. In turn, I would suggest that further research on the relation between the plasma spectrum and TLS noise indicators focuses on the electron density and the plasma temperature.
Another possible reason that this study concludes that there is no correlation between the ratios between the height of key emission peaks in the plasma spectrum during deposition and TLS noise indicators is the difference in the six recipes used inside of the ICP-PECVD in this research. An ICP-PECVD creates different recipes based on its input parameters, resulting in a different deposition. In the six recipes used in this research, all input parameters were changed. This leaves the option open that the conclusion of there being no correlation between the ratios between the heights of emission peaks and TLS noise indicators is caused by the fact that the conditions inside of the ICP-PECVD were different for each recipe. I would suggest that further research on the correlation between the ratios between key emission peaks in the plasma spectrum during deposition and TLS noise indicators defines its difference recipes as recipes in which only one consistent input parameter is changed.

A. Python script

```python
# -*- coding: utf-8 -*-
"""Belangrijke code (1).ipynb

Automatically generated by Colab.

Original file is located at
    https://colab.research.google.com/drive/1uDPRimlUpy7cRn2ctyj1-gvxtq5SqkTu

All used imports and created functions
"""

import pandas as pd
import numpy as np
from scipy.stats import norm
from scipy.optimize import curve_fit
import matplotlib.pyplot as plt
import glob
from scipy.signal import find_peaks
from scipy.stats import zscore
from sklearn.cluster import DBSCAN
wavelength = pd.read_pickle('Pixel_to_wavelength')

def data_prep(location,height,prominence):
    file_paths = glob.glob(location)
    dfs = [pd.read_csv(file, sep='\t') for file in file_paths]
    df_tot = np.zeros(len(dfs[0]["Intensity"]))
    df_avg = np.zeros(len(dfs[0]["Intensity"]))
    for c in range(len(dfs)):
        df_tot=np.add(df_tot,dfs[c]["Intensity"])
    df_avg=df_tot/len(dfs)
    height=height
    prominence=prominence
    peaks, _ = find_peaks(df_avg, height =height, prominence = prominence)
    return df_avg,wavelength[peaks] #call [1] if interested in peaks, else 0

from scipy.special import wofz
def voigt_fit(location,plot):
    def voigt_profile(x, A, mu, sigma, gamma):
        z = ((x - mu) + 1j * gamma) / (sigma * np.sqrt(2))
        return A * np.real(wofz(z)) / (sigma * np.sqrt(2 * np.pi))
    def sum_of_voigt(x, A1, mu1, sigma1, gamma1, A2, mu2, sigma2, gamma2):
        return (voigt_profile(x, A1, mu1, sigma1, gamma1) + voigt_profile(x, A2, mu2, ↩
            sigma2, gamma2))
    data=data_prep(location,10,8)[0] - data_prep('Metingen/Background/*.txt',10,8)[0]
    def voigt_bounds(p0):
        A, mu, sigma, gamma = p0
        return ([0, mu - 5, 0.1, 0],[np.inf, mu + 5, 20, 10])
    def voigt_bounds_sum(p0):
        A1, mu1, sigma1, gamma1, A2, mu2, sigma2, gamma2 = p0
        lower_bounds = [0, mu1 - 5, 0.1, 0,  0, mu2 - 5, 0.1, 0]
```

```
        upper_bounds = [np.inf, mu1 + 5, 20, 10,  np.inf, mu2 + 5, 20, 10]
        return (lower_bounds, upper_bounds)

    dat_range_SiH_2=slice(374,380)
    dat_range_SiH_1= slice(362,372)
    dat_range_SiH_tot=slice(362,380)
    dat_range_SiH_1_hires=slice(36200,37400)
    dat_range_SiH_2_hires=slice(37200,38000)
    dat_range_SiH_tot_hires=slice(36200,38000)
    p0_SiH_1=[80,414,4,2]
    p0_SiH_2=[60,420,4,2]
    p0_SiH_tot = [*p0_SiH_1, *p0_SiH_2]

    dat_range_H=slice(734,742)
    dat_range_H_hires=slice(73400,74200)
    p0_H=[180,656,4,0.2]

    dat_range_H2=slice(655,661)
    dat_range_H2_hires=slice(65500,66100)
    p0_H2=[100,603,4,0.2]

    data_SiH_1=data[dat_range_SiH_1].values
    data_SiH_2=data[dat_range_SiH_2].values
    data_SiH_tot=data[dat_range_SiH_tot]
    data_H=data[dat_range_H].values
    data_H2=data[dat_range_H2].values

    wavelengths_SiH_1=wavelength[dat_range_SiH_1].values
    wavelengths_SiH_2=wavelength[dat_range_SiH_2].values
    wavelengths_SiH_tot=wavelength[dat_range_SiH_tot]
    wavelengths_H=wavelength[dat_range_H].values
    wavelengths_H2=wavelength[dat_range_H2].values

    params_SiH_1, pcov_SiH_1 = curve_fit(voigt_profile, wavelengths_SiH_1, data_SiH_1, p0=p0_SiH_1, bounds=voigt_bounds(p0_SiH_1))
    params_SiH_2, pcov_SiH_2 = curve_fit(voigt_profile, wavelengths_SiH_2, data_SiH_2, p0=p0_SiH_2,bounds=voigt_bounds(p0_SiH_2))
    params_SiH_total, pcov_SiH_total = curve_fit(sum_of_voigt, wavelengths_SiH_tot, data_SiH_tot, p0=p0_SiH_tot, bounds=voigt_bounds_sum(p0_SiH_tot))
    params_H, pcov_H = curve_fit(voigt_profile, wavelengths_H, data_H, p0=p0_H, bounds=voigt_bounds(p0_H))
    params_H2, pcov_H2 = curve_fit(voigt_profile, wavelengths_H2, data_H2, p0=p0_H2, bounds=voigt_bounds(p0_H2))

    err_SiH_1=np.sqrt(np.diag(pcov_SiH_1))
    err_SiH_2=np.sqrt(np.diag(pcov_SiH_2))
    err_H = np.sqrt(np.diag(pcov_H))
    err_H2 = np.sqrt(np.diag(pcov_H2))

    wavelengths_hires_SiH_1 = np.linspace(wavelengths_SiH_1.min(), wavelengths_SiH_1.max()+2, 1200)
    wavelengths_hires_SiH_2 = np.linspace(wavelengths_SiH_2.min()-2, wavelengths_SiH_2.max(), 900)
    wavelengths_hires_SiH_tot = np.linspace(wavelengths_SiH_tot.min(), wavelengths_SiH_tot.max(), 1800)
    wavelengths_hires_H = np.linspace(wavelengths_H.min(), wavelengths_H.max(), 800)
    wavelengths_hires_H2 = np.linspace(wavelengths_H2.min(), wavelengths_H2.max(), 600)

    A1, mu1, sigma1, gamma1, A2, mu2, sigma2, gamma2 = params_SiH_total

    voigt_fit_hires_SiH_1 = voigt_profile(wavelengths_hires_SiH_tot, A1, mu1, sigma1, gamma1)
    voigt_fit_hires_SiH_2 = voigt_profile(wavelengths_hires_SiH_tot, A2, mu2, sigma2, gamma2)


    voigt_sum_fit_hires_SiH = sum_of_voigt(wavelengths_hires_SiH_tot, *params_SiH_total)
    voigt_fit_hires_H = voigt_profile(wavelengths_hires_H, *params_H)
    voigt_fit_hires_H2 = voigt_profile(wavelengths_hires_H2, *params_H2)
```

```
109
110     region_mask_SiH = (wavelengths_hires_SiH_tot >= 412) & (wavelengths_hires_SiH_tot <= 417)
111     max_SiH_region = np.max(voigt_sum_fit_hires_SiH[region_mask_SiH])
112
113     ratio_H_SiH=np.max(voigt_fit_hires_H)/max_SiH_region
114     ratio_H_H2=np.max(voigt_fit_hires_H)/np.max(voigt_fit_hires_H2)
115     ratio_H2_SiH=np.max(voigt_fit_hires_H2)/max_SiH_region
116
117     residuals_SiH = data_SiH_tot.values - sum_of_voigt(wavelengths_SiH_tot, *params_SiH_total)
118     rms_error_SiH = np.sqrt(np.sum(residuals_SiH**2) / (len(wavelengths_SiH_tot) - len(params_SiH_total)))
119
120     residuals_H = data_H - voigt_profile(wavelengths_H, *params_H)
121     rms_error_H = np.sqrt(np.sum(residuals_H**2) / (len(wavelengths_H) - len(params_H)))
122
123     residuals_H2 = data_H2 - voigt_profile(wavelengths_H2, *params_H2)
124     rms_error_H2 = np.sqrt(np.sum(residuals_H2**2) / (len(wavelengths_H2) - len(params_H2)))
125     if plot:
126         plt.figure()
127         plt.plot(wavelengths_hires_SiH_tot,voigt_sum_fit_hires_SiH,label='Fitted sum of Voigts')
128         plt.plot(wavelengths_hires_SiH_tot,voigt_fit_hires_SiH_1,"--",label='Voigt fit 1')
129         plt.plot(wavelengths_hires_SiH_tot,voigt_fit_hires_SiH_2,"--",label='Voigt fit 2')
130         plt.plot(wavelengths_SiH_tot,data_SiH_tot,"o",label='Data points')
131         plt.title('Silylidyne peak')
132         plt.legend()
133         plt.xlabel('Wavelength (nm)')
134         plt.ylabel('Intensity (a.u.)')
135         plt.tight_layout()
136         plt.figure()
137         plt.plot(wavelengths_hires_H,voigt_fit_hires_H,label='Voigt fit')
138         plt.plot(wavelengths_H,data_H,"o",label='Data points')
139         plt.title('Balmer peak')
140         plt.legend()
141         plt.xlabel('Wavelength (nm)')
142         plt.ylabel('Intensity (a.u.)')
143         plt.tight_layout()
144         plt.figure()
145         plt.plot(wavelengths_hires_H2,voigt_fit_hires_H2,label='Voigt fit')
146         plt.plot(wavelengths_H2,data_H2,"o",label='Data points')
147         plt.title('Fulcher peak')
148         plt.legend()
149         plt.xlabel('Wavelength (nm)')
150         plt.ylabel('Intensity (a.u.)')
151         plt.tight_layout()
152     Err_H_SiH=ratio_H_SiH * np.sqrt((rms_error_H / np.max(voigt_fit_hires_H))**2 +(rms_error_SiH / max_SiH_region)**2)
153     Err_H_H2 = ratio_H_H2 * np.sqrt((rms_error_H / np.max(voigt_fit_hires_H))**2 +(rms_error_H2 / np.max(voigt_fit_hires_H2))**2)
154     Err_H2_SiH = ratio_H2_SiH * np.sqrt((rms_error_H2 / np.max(voigt_fit_hires_H2))**2 +(rms_error_SiH / max_SiH_region)**2)
155
156     return ( ratio_H_SiH,ratio_H_H2,ratio_H2_SiH,Err_H_SiH, Err_H_H2,Err_H2_SiH, #0,1,2,3,4,5
157     dat_range_SiH_tot,dat_range_H,  # 6,7
158     voigt_sum_fit_hires_SiH,dat_range_SiH_tot_hires,voigt_fit_hires_H,dat_range_H_hires, #8,9,10,11
159     voigt_fit_hires_H2,dat_range_H2_hires,dat_range_H2, #12,13,14,
160     err_H,err_H2,err_SiH_1) # 15,16,17
161
162 def result_plot(x_data,x_name,y_data,y_name,axlabel,err=None):
163     for i in range(6):
164         n=Recipe_numbers[i]
165         axlabel.scatter(x_data[i],y_data[i],label=f'Recipe {n}')
```

```
        if err is not None:
            axlabel.errorbar(x_data[i],y_data[i],yerr=err[i])
    axlabel.set_ylabel(y_name)
    axlabel.set_xlabel(x_name)
    def lin_fit(y_data,err,x):
        def lin_func(x,A,B):
            return A*x+B
        if err is not None:
            params, pcov = curve_fit(lin_func, x, y_data, sigma=err)
        else:
            params, pcov = curve_fit(lin_func, x, y_data,)
        return params,pcov
    a,b=lin_fit(y_data,err,x_data)[0]
    x_fit=np.linspace(np.min(x_data),np.max(x_data),100)
    y_fit=a*x_fit+b
    std = np.sqrt(np.diag(lin_fit(y_data,err,x_data)[1]))
    y_fit_err = np.sqrt((x_fit**2) * std[0]**2 + std[1]**2 + 2 * x_fit * lin_fit(y_data,err,x_data)[1][0,1] )
    axlabel.plot(x_fit, y_fit, label='Curve fit (with error)', color='deepskyblue')
    axlabel.fill_between(x_fit, y_fit - y_fit_err, y_fit + y_fit_err, color='deepskyblue', alpha=0.3, label='95 % confidence interval')

"""All imported data"""

Recipe_numbers=np.array([2,5,9,10,15,16])

H_content=np.array([0.139493454,0.122704422,0.119656,0.131546523,0.110869883,0.106896645])
R_parameter=np.array([0.33402735,0.409473676,0.357336924,0.363166699,0.372473474,0.550508884])
Void_volume_frac=np.array([18.7183,15.6012,4.5584,14.3621,12.6728,21.496])
Band_gap=np.array([1.7113,1.7143,1.7625,1.5154,1.7927,1.6])
I_850_640=np.array([0.252064808,0.29022615,0.205307863,0.123538421,0.095299256,0.314995959])
Refractive_index=np.array([3.148483402,3.226575078,3.28753614,3.268188999,3.304850987,3.157940549])
Stress=np.array([57.1813604,149.6170963,150.2572112,19.28984156,53.35192947,121.9994303])
Deposition_rate=np.array([10.04335361,37.5936,25.89917355,12.45508593,45.63147854,16.60880347])

"""Plots used in thesis for results"""

ratios_H_SiH=np.zeros(6)
err_H_SiH=np.zeros(6)
for i in range(6):
    n = Recipe_numbers[i]
    if n != 9 :
        ratios_H_SiH[i]=voigt_fit(f'Metingen/Recipe {n}/*.txt',False)[0]
        err_H_SiH[i]=voigt_fit(f'Metingen/Recipe {n}/*.txt',False)[3]
ratios_H_SiH[2]=voigt_fit('Metingen/Recipe 9/Manual fiber/*.txt',False)[0]
err_H_SiH[2]=voigt_fit('Metingen/Recipe 9/Manual fiber/*.txt',False)[3]

x_data=[H_content,R_parameter,Void_volume_frac,Band_gap,I_850_640,Refractive_index,Stress,Deposition_rate]
x_data_names=np.array(['Hydrogen content (%)','R* microstructure parameter (-)','Void volume fraction (%)','Band gap (eV)',\
                       'Ratio I_850/I_640 (-)','Refractive index at 2800 $cm^{-1}$(-)','Stress(Mpa)', 'Deposition rate (nm/min)'])
fig, ax = plt.subplots(4,2,figsize=(13,10))

i=0
for i in range(len(x_data)):
    row = i // 2
    col = i % 2
    result_plot(x_data[i],x_data_names[i],ratios_H_SiH,'$ratio \\frac{H_\\alpha}{SiH}$',ax[row,col],err_H_SiH)

handles, labels = ax[0, 0].get_legend_handles_labels()
fig.legend(handles, labels, loc='upper center', ncol=3, bbox_to_anchor=(0.5, 1.02))
```

```
plt.tight_layout()
plt.subplots_adjust(top=0.87)
plt.savefig('savefig/Results H_SiH', dpi=400, bbox_inches="tight", pad_inches=0.1, transparent = False)

ratios_H2_SiH=np.zeros(6)
err_H2_SiH=np.zeros(6)
for i in range(6):
    n = Recipe_numbers[i]
    if n != 9 :
        ratios_H2_SiH[i]=voigt_fit(f'Metingen/Recipe {n}/*.txt',False)[2]
        err_H2_SiH[i]=voigt_fit(f'Metingen/Recipe {n}/*.txt',False)[5]
ratios_H2_SiH[2]=voigt_fit('Metingen/Recipe 9/Manual fiber/*.txt',False)[2]
err_H2_SiH[2]=voigt_fit('Metingen/Recipe 9/Manual fiber/*.txt',False)[5]

fig, ax = plt.subplots(4,2,figsize=(13,10))
x_data=[H_content,R_parameter,Void_volume_frac,Band_gap,I_850_640,Refractive_index,Stress,Deposition_rate]
x_data_names=np.array(['Hydrogen content (%)','R* microstructure parameter (-)','Void volume fraction (%)','Band gap (eV)',\
                       'Ratio I_850/I_640 (-)','Refractive index at 2800 $cm^{-1}$(-)','Stress(Mpa)', 'Deposition rate (nm/min)'])
i=0
for i in range(len(x_data)):
    row = i // 2
    col = i % 2
    result_plot(x_data[i],x_data_names[i],ratios_H2_SiH,'$Ratio \\frac{Fulcher}{SiH}$',ax[row,col],err_H2_SiH)

handles, labels = ax[0, 0].get_legend_handles_labels()
fig.legend(handles, labels, loc='upper center', ncol=3, bbox_to_anchor=(0.5, 1.02))
plt.tight_layout()
plt.subplots_adjust(top=0.87)
plt.savefig('savefig/Results H2_SiH', dpi=400, bbox_inches="tight", pad_inches=0.1, transparent = False)

"""Plots for showcasing the effect of noise"""

plt.figure(figsize=(10,3))
for i in range(6):
    n = Recipe_numbers[i]
    if n != 9 :
       plt.plot(wavelength,data_prep(f'Metingen/Recipe {n}/*.txt',10,8)[0],label=f'Recipe {n}',alpha=0.4)
plt.plot(wavelength,data_prep(f'Metingen/Recipe {9}/Manual fiber/*.txt',10,8)[0] - data_prep('Metingen/Background/*.txt',10,8)[0], label='Recipe 9')
plt.plot(wavelength,data_prep(f'Metingen/Recipe {9}/Manual fiber/*.txt',10,8)[0],label='Recipe 9')
plt.plot(wavelength,20+data_prep('Metingen/Background/*.txt',10,8)[0],label='Noise with offset 20 a.u.',color='black')

plt.legend()
plt.xlim(573,645)
plt.ylabel('Intensity (a.u.)')
plt.xlabel('Wavelength (nm)')
plt.ylim(0,120)

plt.legend()
plt.grid()
plt.savefig('savefig/Fulcher band with noise', dpi=400, bbox_inches="tight", pad_inches=0.1, transparent = False)
plt.tight_layout()
plt.show()

plt.figure(figsize=(10,3))
for i in range(6):
    n = Recipe_numbers[i]
    if n != 9 :
```

```
        plt.plot(wavelength,data_prep(f'Metingen/Recipe {n}/*.txt',10,8)[0]  - data_prep('Metingen/Background/*.txt',10,8)[0],label=f'Recipe {n}')
plt.plot(wavelength,data_prep(f'Metingen/Recipe {9}/Manual fiber/*.txt',10,8)[0] - data_prep('Metingen/Background/*.txt',10,8)[0], label='Recipe 9')
plt.legend()
plt.xlim(573,645)
plt.ylabel('Intensity (a.u.)')
plt.xlabel('Wavelength (nm)')
plt.ylim(0,120)
plt.legend()
plt.grid()
plt.savefig('savefig/Fulcher band without noise', dpi=400, bbox_inches="tight", pad_inches=0.1, transparent = False)
plt.tight_layout()
plt.show()

"""Plot for showcasing how intensity decreases over time. Measurements of Recipe 10 were imported which were taken at 01-07-2025"""

file_paths = glob.glob('Metingen/Recipe 10/01-7*.txt')
dfs = [pd.read_csv(file, sep='\t') for file in file_paths]
plt.figure()
peaks_lambda=np.empty(len(dfs))
peaks_intensity=np.empty(len(dfs))
for i in range(len(dfs)):
    peak = max(dfs[i]["Intensity"])
    index=np.argwhere(dfs[i]["Intensity"]==peak)[0][0]
#    peaks_lambda[i] = dfs[i]["Wavelength"].iloc[index]
    peaks_intensity[i] = peak


def lin_func(x, a, b):
    return a * x + b

x = np.linspace(0, 35, len(peaks_intensity))
data = np.column_stack((x, peaks_intensity))
dbscan = DBSCAN(eps=4, min_samples=7)
labels = dbscan.fit_predict(data)


unique_labels,counts=np.unique(labels[labels != -1], return_counts=True)
main_cluster=unique_labels[np.argmax(counts)]

inlier_mask=labels== main_cluster
x_good= x[inlier_mask]
y_good =peaks_intensity[inlier_mask]

popt, _=curve_fit(lin_func, x_good, y_good)
slope,intercept=popt
x_line=np.linspace(np.min(x), np.max(x), 100)
y_line=lin_func(x_line, slope, intercept)

plt.figure()
plt.scatter(x, peaks_intensity, color='wheat', label='Outliers')
plt.scatter(x_good, y_good, color='darkorange', label='Density-based clustering inliers')
plt.plot(x_line, y_line, color='deepskyblue', label='Fitted line (inliers only)')

plt.grid()
plt.title('Limitation check intensity decrease')
plt.xlabel("Time (min)")
plt.ylabel("Maximum peak intensity")
plt.legend()
plt.savefig('savefig/Limitation check intensity decrease', dpi=400, bbox_inches="tight", pad_inches=0.1, transparent = False)
plt.show()

"""Other simple plots used in the thesis"""

df_whitelight=data_prep('Metingen/White noise/*.txt',10,8)[0]
```

```
plt.figure(figsize = [12,3])
plt.plot(wavelength,df_whitelight, label = "spectrum",
         linewidth = 0.5, color = 'dodgerblue',
         )
plt.title('White strip lighting measurement')
plt.xlabel('Wavelength (nm)')
plt.ylabel('Intensity (a.u.)')
plt.legend()
plt.savefig('savefig/White strip.png', dpi=400, bbox_inches="tight", pad_inches=0.1, ↩
    transparent = False)
plt.show()

df_background=data_prep('Metingen/Background/*.txt',10,8)[0]
plt.figure(figsize = [12,3])
plt.plot(wavelength,df_background, label = "spectrum",
         linewidth = 0.5, color = 'dodgerblue',
         )
plt.title('Background noise measurement')
plt.xlabel('Wavelength (nm)')
plt.ylabel('Intensity (a.u.)')
plt.legend()
plt.savefig('savefig/Background.png', dpi=400, bbox_inches="tight", pad_inches=0.1, ↩
    transparent = False)
plt.show()

df_argmil=data_prep('Metingen/Argon Milling/*.txt',10,8)[0]
plt.figure(figsize = [12,3])
peaks1, _1 = find_peaks(df_argmil, height =25, prominence = 15)
plt.plot(wavelength,df_argmil, label = "spectrum",
         linewidth = 0.5, color = 'dodgerblue',
         )
plt.plot(wavelength[peaks1], df_argmil[peaks1],
         "x", color = "darkorange", alpha = 0.5,label = "peaks"
        )
plt.title('Argon milling measurement')
plt.xlabel('Wavelength (nm)')
plt.ylabel('Intensity (a.u.)')
plt.legend()
plt.savefig('savefig/Argmil.png', dpi=400, bbox_inches="tight", pad_inches=0.1, ↩
    transparent = False)
plt.show()

df_recipe5=pd.read_csv('Metingen/Recipe 5/24-6 Recipe 5 118.txt',sep='\t')
plt.figure(figsize = [12,3])
peaks1, _1 = find_peaks(df_recipe5["Intensity"], height =15, prominence = 15)
plt.plot(wavelength,df_recipe5["Intensity"], label = "spectrum",
         linewidth = 0.5, color = 'dodgerblue',
         )
plt.plot(wavelength[peaks1], df_recipe5["Intensity"][peaks1],
         "x", color = "darkorange", alpha = 0.5,label = "peaks"
        )

plt.title('White strip lighting measurement')
#plt.ylim(-10,100)
plt.xlabel('Wavelength (nm)')
plt.ylabel('Intensity (a.u.)')
plt.legend()
plt.savefig('savefig/White strip.png', dpi=400, bbox_inches="tight", pad_inches=0.1, ↩
    transparent = False)
plt.show()

voigt_fit('Metingen/Recipe 5/*.txt',True)[0]
```

B. Results values

B.1 Noise indicator values

The Noise indicator values as calculated by J. Heeringa [7]

Recipe:	Duration (min+sec)	Duration (min)	Deposition rate (avg)(nm/min)	Band gap(avg) (eV)
2	38min22sec	38.36666667	10.04335361	1.7113
5	12min30sec	12.5	37.5936	1.7143
9	16min8sec	16.13333333	25.89917355	1.7625
10	35min53sec	35.88333333	12.45508593	1.5154
15	10min29sec	10.48333333	45.63147854	1.7927
16	26min53sec	26.88333333	16.60880347	1.6

Recipe	Stress (avg) (MPa)	Refractive index at 2800 cm^{-1} (-)	Hydrogen content (%)
2	57.1813604	3.148483402	0.139493454
5	149.6170963	3.226575078	0.122704422
9	150.2572112	3.28753614	0.119656
10	19.28984156	3.268188999	0.131546523
15	53.35192947	3.304850987	0.110869883
16	121.9994303	3.157940549	0.106896645

Recipe	Microstructure parameter R* (-)	Ratio I_850/I_640 (-)	Void-volume frac. (%)
2	0.33402735	0.252064808	18.7183
5	0.409473676	0.29022615	15.6012
9	0.357336924	0.205307863	4.5584
10	0.363166699	0.123538421	10.2793
15	0.372473474	0.095299256	12.6728
16	0.550508884	0.314995959	21.496

B.2 Emission peak intensity ratios

Recipe	$\frac{H_\alpha}{SiH}$ peak ratio	$\frac{H_\alpha}{SiH}$ peak ratio error
2	5.64676269	0.4056753
5	2.65286907	0.05436587
9	9.59359956	0.82055545
10	3.81524525	0.48081026
15	7.97246759	0.56063844
16	6.4904014	0.78052214

Table B.1: *The results of the ratios between the emission peaks in the recipes during deposition of the Balmer peak and the Silylidyne peak.*

Recipe	$\frac{\text{Fulcher}}{SiH}$ peak ratio	$\frac{\text{Fulcher}}{SiH}$ peak ratio error
2	2.6468805	0.23081614
5	1.53228155	0.04117226
9	3.41903229	0.30905238
10	3.91345008	0.4897628
15	2.89675944	0.21486277
16	2.7255476	0.3524362

Table B.2: *The results of the ratios between the emission peaks in the recipes during deposition of the Fulcher band peak and the Silylidyne peak.*

C. Mathematical formulas

C.1 Voigt Profile

he Voigt profile $V(x; A, \mu, \sigma, \gamma)$ is the convolution of a Gaussian and Lorentzian function, and is defined as:

$$V(x; A, \mu, \sigma, \gamma) = A \cdot \int_{-\infty}^{\infty} G(x'; \mu, \sigma) \cdot L(x - x'; \mu, \gamma)\, dx' \tag{C.1}$$

$$V(x; A, \mu, \sigma, \gamma) = A \cdot \int_{-\infty}^{\infty} \frac{1}{\sigma\sqrt{2\pi}} e^{-\frac{x'^2}{2\sigma^2}} \cdot \frac{\gamma}{\pi[(x - \mu - x')^2 + \gamma^2]}\, dx' \tag{C.2}$$

It accurately models spectral lines broadened by both Doppler (Gaussian) and pressure or Stark (Lorentzian) effects.

C.2 Residuals

The residuals are the differences between the data points and the fitted values:

$$r_i = y_i - f(x_i; \hat{\mu}, \hat{\sigma}, \hat{A}) \tag{C.3}$$

where $\hat{\mu}, \hat{\sigma}, \hat{A}$ are the fitted parameters.

C.3 Root Mean Squared Error (RMSE)

The RMSE is a measure of the standard deviation of the residuals:

$$\text{RMSE} = \sqrt{\frac{1}{n - p} \sum_{i=1}^{n} r_i^2} \tag{C.4}$$

where:

- n is the number of data points
- p is the number of fitted parameters

C.4 Error Propagation in Ratios

To compute the uncertainty in a ratio of two fitted peak heights, say:

$$R = \frac{H}{S} \tag{C.5}$$

where $H = \max(f_H(x))$ and $S = \max(f_S(x))$, and their respective RMSEs are RMSE_H and RMSE_S, the relative uncertainty in the ratio is:

$$\delta R = R \cdot \sqrt{\left(\frac{\text{RMSE}_H}{H}\right)^2 + \left(\frac{\text{RMSE}_S}{S}\right)^2} \tag{C.6}$$

C.5 DBSCAN

DBSCAN stands for Density-Based Spatial Clustering of Applications with Noise. It groups points that are close together and marks points far from any group as noise. It has two import parameters:

- ε: Radius around each point.
- Min Pts: Minimum number of points to form a dense region.

This means that for a point to be considered inside of a dense region it needs to have an amount of Min Pts inside of its radius ε. After this, it takes the following steps:

1. For each point p, find neighbors within distance ε:

$$N_\varepsilon(p) = \{q \mid \text{dist}(p, q) \leq \varepsilon\} \tag{C.7}$$

2. If $|N_\varepsilon(p)| \geq$ Min Pts, p is a core point.
3. Points reachable through chains of core points belong to the same cluster.
4. Points not reachable from any core point are considered noise.

So basically it checks for any point if it has an amount of Min Pts inside of its ε range. If it does, any other point which is in the neighborhood of this core point is also considered as belonging to the same cluster. Direct density reachability: A point q is directly density-reachable from p if:

$$q \in N_\varepsilon(p) \quad \text{and} \quad |N_\varepsilon(p)| \geq \text{MinPts} \tag{C.8}$$

Clusters = groups of points connected by direct or indirect density reachability. This means that if a point A is a core point and point B is within its range ε. Then if C is within the range of point B (which isn't a core point) it is still considered as part of the cluster.

Bibliography

[1] Anonymous. 2025, Lecture 5: Discrete Spectra of Atoms. https://sites.ualberta.ca/~pogosyan/teaching/ASTRO_122/lect5/lecture5.html

[2] —. 2025, Resonance | Frequency, Amplitude & Wavelength | Britannica. https://www.britannica.com/science/resonance-vibration

[3] Bogaerts, A., Gijbels, R., & Vlcek, J. 1998, Spectrochimica Acta Part B: Atomic Spectroscopy, 53, 1517, doi: https://doi.org/10.1016/S0584-8547(98)00139-6

[4] Buijtendorp, B. 2025, PhD thesis, Delft University of Technology, doi: 10.4233/UUID:50173F5F-CF91-4353-B4A7-2C681FC898D8

[5] Cooper, L. N. 1956, Phys. Rev., 104, 1189, doi: 10.1103/PhysRev.104.1189

[6] Defrance, F., Beyer, A. D., Wheeler, J., Sayers, J., & Golwala, S. R. 2025, Applied Physics Letters, 126, doi: https://doi.org/10.1063/5.0255172

[7] Heeringa, J. 2025, Master's thesis, TU Delft

[8] Kouwenhoven, K., van Doorn, G., Buijtendorp, B., et al. 2024, Phys. Rev. Appl., 21, 044036, doi: 10.1103/PhysRevApplied.21.044036

[9] Markboots. 2011, English: Schematic of a grating spectrometer. https://commons.wikimedia.org/wiki/File:Spectrometer_schematic.svg

[10] Mazzaglia, M., Celona, L., Gammino, S., et al. 2021, Il Nuovo Cimento C, 44, doi: 10.1393/ncc/i2021-21058-9

[11] Nishimura, Y., et al. 2025

[12] NIST. 2025, NIST Atomic Spectra Database Line Form, Tech. rep., National institute of Standards and Technology. https://physics.nist.gov/PhysRefData/ASD/lines_form.html

[13] Oxford Instruments, Inductively Coupled Plasma Chemical Vapour Deposition (ICPCVD). 2025

[14] Reilly, J. T., Walsh, J. M., Greenfield, M. L., & Donohue, M. D. 1992, Spectrochimica Acta Part A: Molecular Spectroscopy, 48, 1459, doi: https://doi.org/10.1016/0584-8539(92)80154-O

[15] Samuell, C., & Corr, C. 2015, Plasma Sources Science and Technology, 24, doi: 10.1088/0963-0252/24/4/045003

[16] T. L. Wilson, S. G. 2018, Millimeter Astronomy (Springer Berlin, Heidelberg), doi: https://doi.org/10.1007/978-3-662-57546-8

[17] Taniguchi, A., Bakx, T. J. L. C., Baselmans, J. J. A., et al. 2022, Journal of Low Temperature Physics, 209, 278–286, doi: 10.1007/s10909-022-02888-5